IEEE Access
Multidisciplinary | Rapid Review | Open Access Journal

Received 15 November 2022, accepted 24 November 2022, date of publication 28 November 2022,
date of current version 5 December 2022.

Digital Object Identifier 10.1109/ACCESS.2022.3225359

RESEARCH ARTICLE

A Novel Control Strategy of Crosswind Disturbance Compensation for Rack-Type Motor Driven Power Steering (R-MDPS) System

DAEYI JUNG AND SORAM KIM
School of Mechanical and Automotive Engineering, Kunsan National University, Gunsan 54150, South Korea

Corresponding author: Daeyi Jung (dyjung@kunsan.ac.kr)

This work was supported in part by the Ministry of Trade, Industry and Energy, an Industrial Technology Innovation Project, "Development for Steering Thrust 3500 kgf Class Integrated Electric Power Steering System (MDPS)," under Project P0013843; and in part by the Korea Institute for Advancement of Technology (KIAT) through the Korea Government (MOTIE) under Grant P0013851 ("Development of a Auxiliary Axle Steering for 10-Ton Class Electro-Hydraulic Synchronous Steering System").

ABSTRACT The wind suddenly blown to the side of the car (i.e, cross-wind effect) is considered as one of the major lateral disturbances, which causes the unstable motion of the vehicle and the persistent driving fatigue for the driver who tracks the desired travel path. In particular, a commercial vehicle having a large side area is greatly affected by this effect. Therefore, many related automotive/car manufacturers still wish to equip their Advanced Driving Assistant System (ADAS) with the crosswind disturbance compensation control system. Meanwhile, in recent advanced vehicle systems, a rack-type motor-driven power steering (R-MDPS) system is more widely used than a column-type MDPS (C-MDPS) due to the structural advantage and the effective steering assistance. Recognizing those two issues, this paper investigates a novel anti-control and estimation strategy of crosswind disturbance for the R-MDPS system of vehicles with non-negligible side surfaces. Specifically, an adaptive disturbance observer (D.O.B) has been proposed to estimate the crosswind effect. Furthermore, using optimal control theory, the compensation control system is designed to assist the driver in two possible situations. One is for when the driver continues to steer the vehicle under the effect of the crosswind, and the other is for when the driver temporarily loses steering control due to the effect. In addition, the control mode selection conditions between two controls are clearly presented to maximize the efficiency and performance of the proposed control system, which has not yet been sufficiently investigated. Finally, the effectiveness of the proposed control system has been evaluated based on Simulink/Carsim Co-simulation and HILS environments.

INDEX TERMS Lateral disturbance compensation control, rack-type motor driven power steering system (R-MDPS), crosswind effect, vehicle dynamics, disturbance observer (D.O.B), Carsim, hardware-in-the-loop simulation (HILS).

I. INTRODUCTION

The effect of crosswinds is one of the major problems associated with the vehicle safety and stability. Occasionally, due to this effect, SUVs or commercial vehicles with a high center of gravity and a large side area may overturn, and a passenger car may be trapped in a side slip motion. Many car accidents have been reported at wind-exposed structure such as a bridge [1]. According to [2], the lateral disturbance by crosswind is insignificant at low speed, however strong crosswind, it can cause the vehicle out of its lane or make it overturn. This lateral disturbance can reduce the driver's steering control in driving situations, and can be an apparent threat to the safety of the driver. Reference [3] investigated the

The associate editor coordinating the review of this manuscript and approving it for publication was Xiwang Dong.

stability of the vehicle and the course deviation under strong crosswind. In recent years, as vehicles have adopted higher vehicle speeds and are designed to be lightweight for greater fuel economy, [4] has provided the fact that the likelihood of crosswind-related accidents has increased. Therefore, the estimation/anti-control strategy of crosswind effect have been proposed by several previous studies. Regarding the aspect of estimation, [5], [6], [7] proposed the techniques for estimating this crosswind effect on the vehicle without any sensor directly measuring aerodynamic effect. Reference [5] used 2-D.O.F bicycle model-based linear observer to estimate the effect while [6], [7] used Kalman filter for estimating a tire self-aligning torque and the lateral disturbance. Furthermore, the anti-crosswind control strategies and related investigations have been proposed in [8], [9], [10], [11], [12], and [13]. Reference [8] designed the switching control between reverse control strategy and obverse control one to reduce the effect on the vehicle. Here, reverse control strategy is responsible for active steering control while obverse control is adopted to provide steering assistance. Reference [9] and [10] addressed the control strategy using the overlay torque of assistant motor as a control input which improves the human steering behavior under the lateral disturbance, a cross-wind effect and a road bank angle. Especially, [10] discussed the effectiveness of proposed lateral compensation algorithm based on a fully-equipped simulator interacting with a human driver. Reference [11] designed a reversing assistance strategy using a flexible-PID control scheme, adopting to avoid excessive lateral driving in the absence of driver input. Reference [12] used the disturbance observer (DOB) and H-infinity optimal control scheme to reject the lateral disturbance. Reference. [13] designed a minimally configured hardware-in-the-loop simulator of electrical power steering system and investigated human driver interaction on crosswind effect. Finally, this work proposed the approximate range of overlay steering torque for the crosswind effect. Reference [14] and [15] proposed the crosswind stabilization using the proper braking force via ESP. Specifically, the brakes are applied on the wheels opposite of the ones facing the crosswind (i.e, torque vectoring) to reduce the lateral deviation of vehicle.

More advanced control system, so-called Lane-keeping system, for the lateral disturbance have been developed with the vision system to detect the lane marker of road [16], [17], [19]. Reference [16] developed a distance to line crossing (DLC) based computation of time to line crossing (TLC) as a lane departure indicator. Reference [17] designed a lane keeping controller for motorcycles using 4-D.O.F model and optimal control. Reference [18] described the design and practical implementation of a lane departure avoidance assistance for passenger vehicles based on a state feedback dynamic controller. Here, Lyapunov theory and bilinear matrix inequalities including bounds in the control input and constraints for poles clustering are used to minimize the reachable set of the vehicle after activation of the assistance. Reference [19] presented a semi-autonomous lane departure assist system keeping the vehicle in the lane for the lateral disturbances. Meanwhile, recently, the R-MDPS is widely used for the steering system because a motor attached to the rack can deliver the assistance torque more effectively and directly than C-MDPS. Accordingly, automakers are focusing on the production of R-MDPS systems and trying to install these into more vehicles. Reference [20], [21], and [22] presented the relevant works for R-MDPS modeling and control design. Reference [20] focuses on the estimation of the steering rack force with real-time capable algorithms using a nonlinear friction compensation module and a linear disturbance observer. The estimation algorithm is validated by a real prototype car. Reference [21] modeled rack-assisted EPS mathematically and proposed H∞-controller to follow a reference steering torque quickly and accurately. Reference [22] applied R-MDPS to the heavy truck and proposed control strategy for analyzing control system with a dynamic vehicle system in Simulink/Trucksim co-simulation environment.

Although [8], [9], [10], [11], [12] proposed various crosswind effect compensation control strategy, the complete and integral solution of control system for the crosswind effect has not yet been addressed. Under the influence of crosswind, [8] and [11] consider only the situation without human driver input (i.e, a driver loses steering control due to the effect) while [9], [10], [12] investigated the proposed control system for when a human driver still steers the vehicle. Furthermore, none of them explored the criteria whether human driver involves or not for this situation. Although the braking-based cross stabilization in [14] and [15] induces the direct and effective counteracting for crosswind, the drivers often feel less comfortable than the steering-based control approaches and it causes energy wasted and tire wear due to the sudden braking.

Also, even without any lane-keeping system in [16], [17], [18], and [19], some car manufacturers still and at least want to equip the driver assisting lateral disturbance control system in their low-cost vehicles or commercial ones by using existing sensors. And, the investigation of an anti-control system for the crosswind in the R-MDPS system has been limited. Therefore, this paper proposed a novel control strategy of crosswind disturbance compensation for the rack-type motor-driven power steering (R-MDPS) system using the existing sensor values from the vehicle. Specifically, the adaptive disturbance observer (D.O.B) is designed to estimate the crosswind effect in terms of both the magnitude and direction based on the ideas of [5], [6], [7]. Furthermore, compared to [8], [9], [10], [11], and [12], using optimal control theory, the control system is designed to assist the driver in both situations. One is for when the driver continues to steer the vehicle under the effect of the crosswind, and another is for when the driver temporarily loses steering control due to the effect. Also, the condition whether human driver involves or not for this situation, the control mode selection strategy between two controls, is clearly addressed based on the vehicle stability and driver effort under the undesired crosswind effect. Finally, the effectiveness of the proposed control system has been evaluated based on the Simulink/Carsim

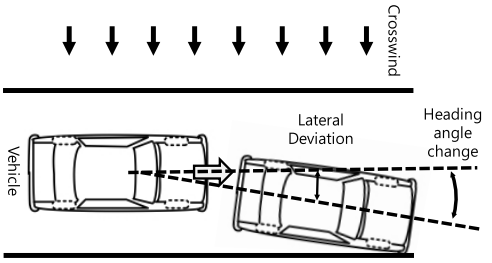

FIGURE 1. The heading angle change and the lateral deviation of vehicle due to crosswind effect.

Co-simulation and HILS environments here. **Section. II** and **III** present the problem formula and design of the disturbance observer for estimating the crosswind effect, respectively. **Section. IV** and **V** describe the R-MDPS system and lateral disturbance control strategy. Next, the simulation results and conclusions are followed.

II. PROBLEM FORMULATION

This section formulates the problem to be addressed in this study. First, let's consider a vehicle affected by one of the major lateral disturbances, a crosswind, as shown in Fig. 1. As a result, the vehicle usually experiences the heading angle change and the lateral deviation from the desired path-line, which may lead to an unexpected car accident [1], [2], [3], [4]. Even if the car avoids serious situations, the driver's fatigue in these undesirable situations increases as the driver has to make constant steering efforts [9], [10].

To meet high standards for estimation and control, this section presents the requirements for the overall estimation/control scheme. Specifically, two important actions are required. One is an accurate estimate of the crosswind effect without any additional sensors such as Lidar or vision sensors, which means it requires an advanced observer to estimate the effect of the crosswind. And the other is the effective anti-control strategy of the crosswind effect via a R-MDPS steering system for two possible cases, a driver's intervention and no intervention. Furthermore, along with control system, proper detection and control mode selection conditions between two cases should be presented.

A. REQUIREMENT OF ESTIMATION SYSTEM

Based on the sensor values available from existing sensors in vehicles without adding any other sensors directly measuring wind effect, the direction and magnitude of crosswind should be estimated. Thus, this study employs the lateral acceleration and yaw rate for the estimation process, which are already available from the existing sensors/ECU. The estimation result for the crosswind effect should include the least transient responses such as small overshoot and appropriate rising time because they will be directly used in the control system, resulting in smooth and quick compensation without interfering the driver's intention excessively.

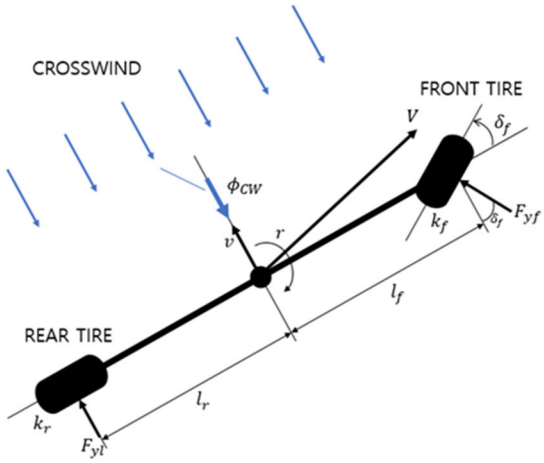

FIGURE 2. 2-D.O.F bicycle model with a cross-wind effect.

B. REQUIREMENT OF CONTROL SYSTEM

Two control modes should be designed for this study. While the first control mode is for the case when a driver constantly counter-steer against crosswind effect, the second is for the one where a driver lose the steering control temporarily due to the effect. The first control mode focuses on reducing the steering effort (i.e, steering wheel torque delivered by a driver), relying on the driver for steering the vehicle properly. On the other hands, the second control momentarily overrides the vehicle not to be seriously deviated from the desired travel path-line (i.e, usually straight road). However, it should be noted that the second control is not an autonomous function to enhance the vehicle to track the desired path-line forever and assumes to hand over the steering control to the driver after a short period of override control. This might be more useful if collaborated with a warning alarming system in ADAS. In addition, the control mode selection strategy is required to properly choose the control mode between the first control and the second one. This implies that a specific condition to grasp the status of both the vehicle and a driver under the influence of the crosswind should be addressed.

III. DISTURBANCE OBSERVER DESIGN FOR CROSS-WIND ESTIMATION

This section presents the design of model-based disturbance observer for the estimation of crosswind effect on the vehicle. Specifically, the 2-D.O.F bicycle model under the effect of crosswind is introduced and then, based on the model, the design of adaptive disturbance observer and the gain selection of designed observer are discussed here.

A. 2-D.O.F BICYCLE MODEL TOGETHER WITH CROSS-WIND EFFECT

In Fig. 2, we introduced 2-D.O.F bicycle model together with crosswind effect for the design of the disturbance observer to estimate the crosswind effect.

TABLE 1. The parameter values of the 2-D.O.F bicycle model.

Parameters	Values
m	2,750 (kg)
I_z	2,282 (kgm^2)
l_f	1.5 (m)
l_r	1.35 (m)
k_f	33,000 (N/rad)
k_r	34,000 (N/rad)

The state-space model for 2-D.O.F bicycle model with a cross-wind effect are given by,

$$\begin{bmatrix} \dot{v}(t) \\ \dot{r}(t) \end{bmatrix} = \begin{bmatrix} a_{11} & a_{12} \\ a_{21} & a_{22} \end{bmatrix} \begin{bmatrix} v(t) \\ r(t) \end{bmatrix} + \begin{bmatrix} b_1 \\ b_2 \end{bmatrix} \delta_f(t) + \begin{bmatrix} 1 \\ 0 \end{bmatrix} \phi_{cw}(t) \quad (1)$$

$$\begin{bmatrix} a_y(t) \\ r(t) \end{bmatrix} = \begin{bmatrix} a_{11} & a_{12}+V \\ 0 & 1 \end{bmatrix} \begin{bmatrix} v(t) \\ r(t) \end{bmatrix} + \begin{bmatrix} b_1 \\ 0 \end{bmatrix} \delta_f(t) + \begin{bmatrix} 1 \\ 0 \end{bmatrix} \phi_{cw}(t) \quad (2)$$

where $v(t)$ and $r(t)$ are the vehicle's lateral velocity and yaw rate, respectively. And, $\delta_f(t)$ is the front steering wheel angle and $\phi_{cw}(t)$ is the lateral disturbance effect caused by the crosswind, which is the lateral aerodynamic force (denoted as $F_{aero.y}$) acting on the side of the vehicle divided by the vehicle mass m (i.e, $F_{aero.y}/m$). Also, V is the longitudinal velocity of vehicle. Here, we neglect the moment that causes the vehicle's yaw motion due to ϕ_{cw} because this simplification does not degrade the estimation performance and reduces the complexity of observer. Each component $a_{11}, a_{12}, a_{21}, a_{22}$, b_1 and b_2 in (1) and (2) are summarized by,

$$a_{11} = -\frac{2(k_f + k_r)}{mV}, \quad a_{12} = -\frac{2(k_f l_f - k_r l_r)}{mV} - V$$
$$a_{21} = -\frac{2(k_f l_f - k_r l_r)}{I_z V}, \quad a_{22} = -\frac{2(k_f l_f^2 + k_r l_r^2)}{I_z V}$$
$$b_1 = \frac{2k_f}{m}, \quad b_2 = \frac{2k_f l_f}{m}$$

The parameters, l_f and l_r, are the distance from the front wheel to vehicle's center of gravity (C.G) and the distance from the rear wheel to C.G, respectively. And, m and I_z are the mass and moment inertia of the vehicle. In addition, k_f and k_r are the cornering stiffness by tire/road force, respectively. Those parameter values used for the 2-D.O.F bicycle model are listed in **Table 1** and will be used throughout the paper, unless specified otherwise.

B. DESIGN OF ADAPTIVE DISTURBANCE OBSERVER

The specific design of disturbance observer is presented here. It is well known that the lateral acceleration $a_y(t)$ and the yaw rate $r(t)$ are the output signals available via a senor/ECU in a vehicle. Meanwhile, the control system (will be discussed in **Section.V**) demands the lateral velocity $v(t)$, the yaw rate $r(t)$, as well as the crosswind effect ϕ_{cw}. Here, both $v(t)$ and ϕ_{cw} are not directly available from sensors so that the proposed observer should estimate those two and be designed to fulfill this purpose. Therefore, in order to simultaneously estimate the disturbance ϕ_{cw} and $v(t)$, an augmented state-space model with an additional state ϕ_{cw} based on (1) and (2) is proposed below,

$$\dot{X}_e = \boldsymbol{A}_e \boldsymbol{X}_e + \boldsymbol{B}_e \boldsymbol{u} + \boldsymbol{E}_e d \quad (3)$$

$$\begin{bmatrix} \dot{v} \\ \dot{r} \\ \dot{\phi}_{cw} \end{bmatrix} = \begin{bmatrix} a_{11} & a_{12} & 1 \\ a_{21} & a_{22} & 0 \\ 0 & 0 & 0 \end{bmatrix} \begin{bmatrix} v \\ r \\ \phi_{cw} \end{bmatrix} + \begin{bmatrix} b_1 \\ b_2 \\ 0 \end{bmatrix} \delta_f + \begin{bmatrix} 0 \\ 0 \\ 1 \end{bmatrix} \dot{\phi}_{cw}$$

$$\boldsymbol{y}_e = \boldsymbol{C}_e \boldsymbol{X}_e + \boldsymbol{D}_e \boldsymbol{u} \quad (4)$$

$$\begin{bmatrix} a_y \\ r \end{bmatrix} = \begin{bmatrix} a_{11} & a_{12} & V_1 \\ 0 & 1 & 0 \end{bmatrix} \begin{bmatrix} v \\ r \\ \phi_{cw} \end{bmatrix} + \begin{bmatrix} b_1 \\ 0 \end{bmatrix} \delta_f$$

Based on (3) and (4), the disturbance observer can be given by,

$$\dot{\hat{X}}_e = \boldsymbol{A}_e \hat{X}_e + \boldsymbol{L}\left(\boldsymbol{y}_e - \hat{y}_e\right) + \boldsymbol{B}_e \boldsymbol{u} + \boldsymbol{E}_e \hat{d}$$
$$\hat{\boldsymbol{y}}_e = \boldsymbol{C}_e \hat{X}_e + \boldsymbol{D}_e \boldsymbol{u} \quad (5)$$

where, $\widehat{\boldsymbol{X}}_e = \begin{bmatrix} \hat{v} & \hat{r} & \hat{\phi}_{cw} \end{bmatrix}^T \in \mathbb{R}^{3\times 1}$, $\hat{y} = \begin{bmatrix} \hat{a}_y \hat{r} \end{bmatrix} \in \mathbb{R}^{2\times 1}$, and $\mathbf{L} \in \mathbb{R}^{3\times 2}$ are the estimates of actual $\boldsymbol{X}_e = [v\ r\ \phi_{cw}]^T$, the estimates of $\boldsymbol{y}_e$ as well as the gain of observer, respectively. And, $\hat{d} \in \mathbb{R}$ is the estimate of $d = \dot{\phi}_{cw}$ in (3).

The calculation of $\hat{d}$ in (5) is given by,

$$\hat{d} = \int_{t0}^{tf} w\left(\boldsymbol{y}_e - \hat{y}_e\right)^T \boldsymbol{C}_e \boldsymbol{E}_e \, dt \quad (6)$$

where $w > 0 \in \mathbb{R}$ is a positive constant. Also, (6) is equivalent to $\dot{\hat{d}} = w\left(\boldsymbol{y}_e - \hat{y}_e\right)^T \boldsymbol{C}_e \boldsymbol{E}_e$.

Theorem 1: The error between the actual states $\boldsymbol{X}_e$ and the estimates $\hat{\boldsymbol{X}}_e$ is converged to zero, which implies that the error dynamics (9) is asymptotically stable at origin, if the gain matrix $\boldsymbol{L}$ is designed such that $\max\left(\mathrm{Re}\left(\lambda_i\left(\boldsymbol{A}_e - \boldsymbol{L}\boldsymbol{C}_e\right)\right)\right) < 0$, where the notations $\lambda_i(\cdot)$ and $\mathrm{Re}(\cdot)$ represent the eigenvalues of $(\cdot)$ and the real part of $(\cdot)$, respectively.

Proof: Selecting the following candidate Lyapunov function,

$$V(t) = \frac{1}{2}\boldsymbol{e}^{\boldsymbol{T}} \boldsymbol{C}_e^{\boldsymbol{T}} \boldsymbol{C}_e \boldsymbol{e} + \frac{1}{2} w^{-1} d_e^2 \quad (7)$$

where, $\boldsymbol{e} = \boldsymbol{X}_e - \hat{X}_e \in \mathbb{R}^{3\times 1}$ and $d_e = d - \hat{d} \in \mathbb{R}$. And, $\boldsymbol{C}_e^{\boldsymbol{T}} \boldsymbol{C}_e > 0 \in \mathbb{R}^{3\times 3}$.

Taking the derivative of $V(t)$ with respect to a time t yields,

$$\dot{V}(t) = \boldsymbol{e}^{\boldsymbol{T}} \boldsymbol{C}_e^{\boldsymbol{T}} \boldsymbol{C}_e \dot{\boldsymbol{e}} + w^{-1} d_e \dot{d}_e \quad (8)$$

Assuming that the true $\dot{d} = \ddot{\phi}_{cw}$ is assumed to be zero, we have $\dot{d}_e = -\dot{\hat{d}}$. It is reasonable if the derivative of ϕ_{cw} with respect of a time (i.e, $d = \dot{\phi}_{cw}$) is finite. Meanwhile, the error dynamics can be obtained by subtracting (5) from (3) and given by,

$$\dot{\boldsymbol{e}} = [\boldsymbol{A}_e - \boldsymbol{L}\boldsymbol{C}]\,\boldsymbol{e} + \boldsymbol{E}_e d_e \quad (9)$$

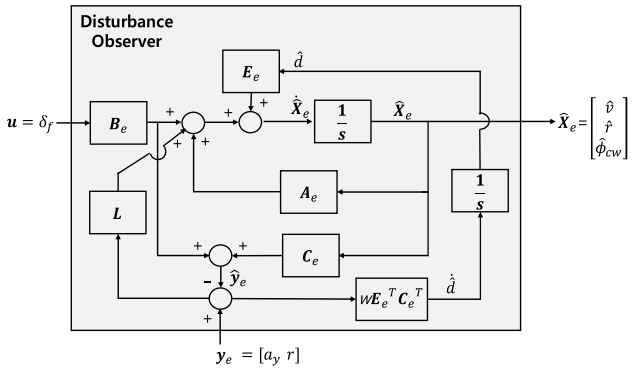

FIGURE 3. Structure of disturbance observer.

Therefore, applying the condition $\dot{d}_e = -\dot{\hat{d}}$ into (8) and substituting (9) into (8) yield,

$$\dot{V}(t) = \boldsymbol{e}^T \boldsymbol{C}_e^T \boldsymbol{C}_e \left[\boldsymbol{A}_{ce}\boldsymbol{e} + \boldsymbol{E}_e d_e\right] - w^{-1}\dot{\hat{d}} d_e \tag{10}$$

where $\boldsymbol{A}_{ce} = \boldsymbol{A}_e - \boldsymbol{L}\boldsymbol{C} \in \mathbb{R}^{3\times 3}$.

Furthermore, (10) becomes,

$$\dot{V}(t) = \boldsymbol{e}^T \boldsymbol{C}_e^T \boldsymbol{C}_e \boldsymbol{A}_{ce}\boldsymbol{e} + \left[\boldsymbol{e}^T \boldsymbol{C}_e^T \boldsymbol{C}_e \boldsymbol{E}_e - w^{-1}\dot{\hat{d}}\right] d_e \tag{11}$$

Applying (6) into (11) yields $\dot{V}(t) = \boldsymbol{e}^T \boldsymbol{C}_e^T \boldsymbol{C}_e \boldsymbol{A}_{ce}\boldsymbol{e}$. Finally, we have $\dot{V}(t) < 0$ because $\max \mathrm{Re}\left(\lambda_i \left(\boldsymbol{C}_e^T \boldsymbol{C}_e \boldsymbol{A}_{ce}\right)\right) < 0$ due to $\max\left(\mathrm{Re}\left(\lambda_i\left(\boldsymbol{A}_{ce}\right)\right)\right) < 0$. Consequently, $\boldsymbol{e} \to \boldsymbol{0}$ (i.e, asymptotically stable). Based on $\boldsymbol{e} \to \boldsymbol{0}$ and (9),we can achieve that $d_e = d - \hat{d} \to 0$ under the condition of persistence excitation. The proof is completed ■

The structure of observer is described in Fig. 3. The estimates of observer, $\hat{\boldsymbol{X}}_e$, will be used in the lateral disturbance compensation control presented in **Section.V**.

C. GAIN SELECTION OF DISTURBANCE OBSERVER

In addition, designing the proper gain of observer $\boldsymbol{L}$ in (5) is essential to achieve the desired estimation performance. In order to do this task, we will use the pole-placement technique, which implies that the desired poles of the proposed observer should be appropriately selected. Before choosing the desired pole, the poles of the open-loop system (represented by $\boldsymbol{A}_e$ in (3)) should be investigated because it allows us to make a wise choice accommodating the characteristics of original system some extent. Thus, based on $\boldsymbol{A}_e$, the corresponding characteristic equation of open-loop system is given by,

$$|s\boldsymbol{I}_{3\times 3} - \boldsymbol{A}_e| = s\left(s^2 + 2\zeta\omega_n s + \omega_n^2\right) = 0 \tag{12}$$

where, $\omega_\mathrm{n} = \sqrt{a_{11}a_{22} - a_{12}a_{21}}$ and $\zeta = -(a_{11} + a_{22})/(2\sqrt{a_{11}a_{22} - a_{12}a_{21}})$ together with the condition $a_{11}a_{22} - a_{12}a_{21} > 0$ and $a_{11} + a_{22} < 0$.

As shown in (12), it should be noted that the open-loop system is unstable since one of roots is zero, which is marginally stable (i.e, unstable in the aspect of stability). However, it can be easily seen from (12) that the rest of roots $\mathrm{s}_{1.2} = -\zeta\omega_\mathrm{n} \pm \omega_\mathrm{n}\sqrt{1-\zeta^2}j$ lie on the left half side of Re-Im plane (i.e, stable), where j is an imaginary number. Those roots are described in Fig. 4.

Remarks 1 (Selection for Desired Poles): The unstable root $\mathrm{s} = 0$ of open-loop system should be re-located to another thus, in this study, the three possible cases have been considered such as $\mathrm{s} = -\mu_\mathrm{i} < Re\,(\mathrm{s}_{1.2}) = -\zeta\omega_\mathrm{n}$ for $i = 1,2,3$, where the unstable root is moved away from both the origin (i.e, s=0) and located at the position with certain margin of Re $(\mathrm{s}_{1.2})$. However, it should be mentioned that we decided to keep the two stable roots of the open-loop system in order to accommodate the characteristics of the original system with some margin. Therefore, $\mu_1 = -1.05\zeta\omega_\mathrm{n}$, $\mu_2 = -1.4\zeta\omega_\mathrm{n}$, and $\mu_3 = -4.0\zeta\omega_\mathrm{n}$ are chosen. The three possible roots $-\mu_\mathrm{I}$ are also specified in Fig. 4.

Based on **Remarks. 1**, the desired poles (denoted as $\mathrm{s}_{m.d}$ for $m = 1,2,3$) are determined by,

$$\begin{aligned} s_{m.d} &= -\zeta\omega_n \pm \omega_n\sqrt{1-\zeta^2}j \; for \; m = 1, 2 \\ s_{3.d} &= -\mu_i \text{ for } i = 1, 2, 3 \end{aligned} \tag{13}$$

The corresponding gain of observer $\boldsymbol{L}$ can be obtained by matching the desired poles $\mathrm{s}_{m.d}$ in (13) with the roots of characteristic equation for the closed-loop system represented by $\boldsymbol{A}_{ce} = \boldsymbol{A}_e - \boldsymbol{L}\boldsymbol{C}$ such as $|\mathrm{s}\mathbf{I}_{3\times 3} - \boldsymbol{A}_{ce}| = (s - \mathrm{s}_{1.d})(s - \mathrm{s}_{2.d})(s - \mathrm{s}_{3.d})$.

Using the parameters in **Table 1** and (3) through (6), for three cases μ_i, the time-domain responses of estimate ϕ_{cw} for unit step input via the proposed observer are described in Fig. 4(b). According to the results of Fig. 4(b), it is found that the rising times (t_r) are 0.81 (sec.) for the case1 (i.e, $\mu_1 = -1.05\zeta\omega_\mathrm{n}$), 0.51 (sec.) for the case2 (i.e, $\mu_2 = -1.5\zeta\omega_\mathrm{n}$), and 0.45 (sec.) for the case3 (i.e, $\mu_3 = -4.5\zeta\omega_\mathrm{n}$). Also, based on Fig. 4(b), both case1 and case2 show the responses similar to the 1st order response without overshoot while the case 3 exhibits the 2nd order response (because μ_3 is located away almost five times from two other desired poles $\mathrm{s}_{m.d}$ for $m = 1, 2.$). Depending on the requirements of the observer in **Section.II**, the overshoot of estimate for ϕ_{cw} should be minimized or avoided since it will be directly provided to the control system. In this way, the driver will experience the least uncomfortable steering control performed by the control system (i.e. smooth compensation may not be achieved if the estimate contains an excessive overshoot).

In addition, the estimation of crosswind must be quickly performed because the control system should properly respond to the effects (i.e, an appropriate rising time is required).

Therefore, we selected the case2 (i.e, $\mathrm{s}_{3.\mathrm{d}} = -1.4\zeta\omega_\mathrm{n}$) for this study, which exhibits an adequate rising time without overshoot. However, if a faster response is desired, the $\mathrm{s}_{3.d}$ can be arbitrarily selected from the range of in between $-1.4\zeta\omega_\mathrm{n}$ and $-4.0\zeta\omega_\mathrm{n}$.

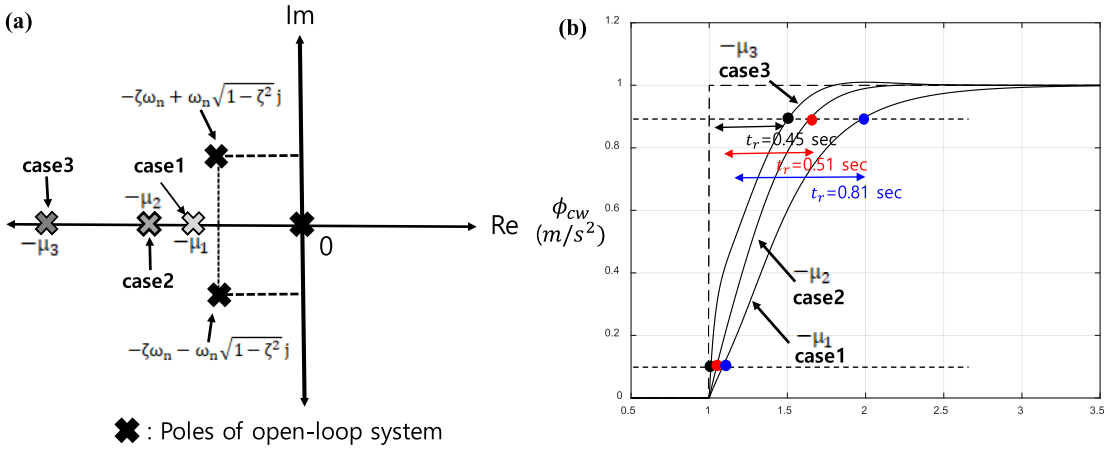

FIGURE 4. Locations of poles for open-loop system and desired poles, and corresponding time-domain responses for step input (a) Poles for open-loop system and desired poles (b) Time-domain responses of estimate ϕ_{cw} for unit step input.

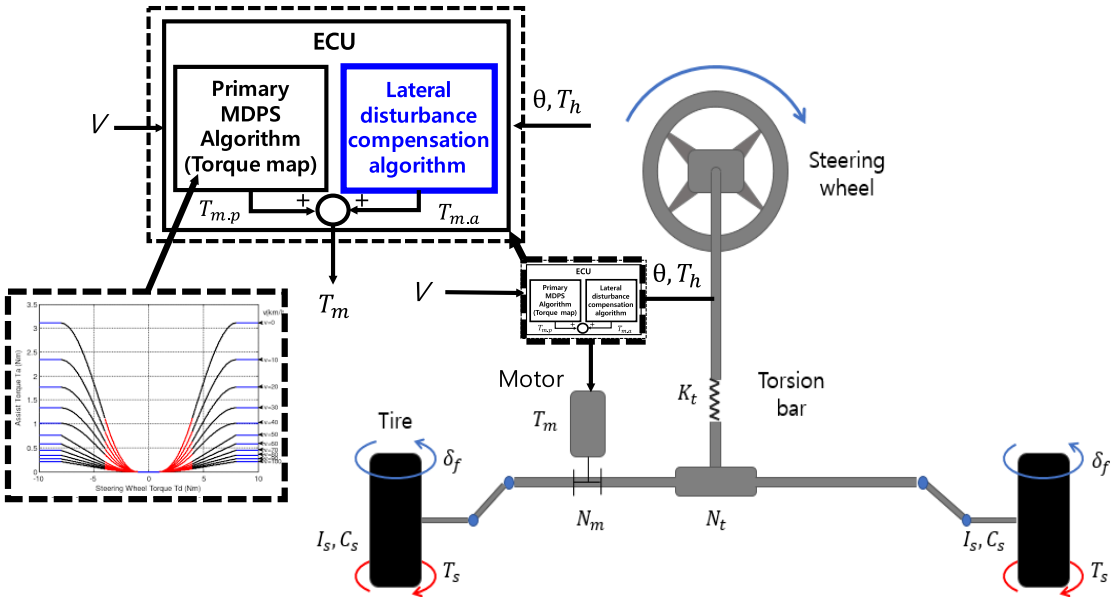

FIGURE 5. Rack-type MDPS (R-MDPS) system with lateral disturbance control.

IV. RACK-TYPE MDPS SYSTEM AND ASSISTANT TORQUE

In this section, the mathematical model of R-MDPS system has been introduced. As shown in Fig. 5, the assistance motor controlled by an ECU is attached to the rack of steering system (instead of column) for reducing human driver's steering effort. The assistance level is determined by the assistant torque map embedded in the ECU, depending on the inputs, vehicle longitudinal speed and steering wheel torque/angle. In addition, for the purpose of this study, the lateral disturbance compensation algorithm should be equipped with the ECU. Therefore, under the normal driving, the primary MDPS algorithm determines the assistant torque of motor according to torque map. On the other hands, under the influence of crosswind effect, an additional torque determined by lateral disturbance compensation algorithm is required to assist a driver to steer the vehicle properly. This leads that, for some cases, the sum of those two torques will be the desired torque of the motor.

A. MATHEMATICAL MODEL OF R-TYPE MDPS SYSTEM

Based on model depicted in Fig. 5, the equation-of-motions (E.O.M) for the R-MDPS system is given by,

$$I_s\ddot{\delta}_f(t) + C_s\dot{\delta}_f(t) = T_{self}(t) + N_m T_m(t) + N_t T_h(t) \quad (14)$$

where $\delta_f(t)$ is a front steering angle which can be possibly measured by an encoder attached to the motor. Also, N_t, N_m, I_s, and C_s are respectively the steering gear ratio, the motor gear ratio, the equivalent moment of inertia as well as the damping coefficient of the steering system. And, T_m and T_h represent a torque transmitted by the motor and a

TABLE 2. Parameter values of the steering system.

Parameters	Values
I_s	5.2 (kgm^2)
C_s	0.01 $(Nm/rad/s)$
N_t	21
N_m	5
K_t	120 (N/rad)
ξ	0.07 (m)

steering wheel torque delivered by a human driver, respectively. Although more detailed model in [18] and [19] can be used for this study, (14) still represents the essence of steering system and is sufficient for the design of desired control system.

The steering wheel torque can be measured by a torsional bar using the angular difference between a steering wheel angle and a front wheel steering angle, δ_f,

$$T_h(t) = K_t\left(\theta(t) - N_t\delta_f(t)\right) \tag{15}$$

where, $\theta(t)$ represents the steering wheel angle and can be obtained by a steering wheel sensor (i.e, a rotational encoder senor). And, K_t is the stiffness coefficient of tensional bar. The equivalent self-align moment, $T_{self}(t)$, occurred at tire/ground is approximately calculated by,

$$T_{self}(t) = 2\xi k_f\left(\frac{v(t)}{V(t)} + \frac{l_f}{V(t)}r(t) - \delta_f(t)\right) \tag{16}$$

where ξ is the trail length of front tire. The parameter values of (14) through (16) for this study are listed in **Table 2** and will be used throughout here unless specified otherwise.

B. ASSISTANT TORQUE OF MOTOR IN R-TYPE MDPS SYSTEM

As shown in Fig. 5, the motor torque $T_m(t)$ can be divided into two parts, the primary assistant torque (denoted as $T_{m.p}(t)$) according to the magnitude of $T_h(t)$ and the additional torque (denoted as $T_{m.a}(t)$) for the crosswind effect. Hence, we have $T_m(t) = T_{m.p}(t) + T_{m.a}(t)$. Also, it is well known that $T_{m.p}(t)$ depends on $T_h(t)$ and the longitudinal velocity V. In other words, $T_{m.p}(t) = f(T_h, V)$ where $f(T_h, V)$ is so-called assistant torque map. If the vehicle is driven at a constant speed, it can be approximately assumed that $T_{m.p}(t) \approx \alpha T_h(t)$ (i.e, $T_{m.p}(t)$ is linearly related to $T_h(t)$) in the range that $T_h(t)$ is larger than a certain value such as $|T_h(t)| > T_{h.c} \in \mathbb{R}$, and $\alpha \in \mathbb{R}$ is an amplified constant which is the slope of curve line in an assistant torque map. Therefore, $T_m(t)$ can be expressed by,

$$T_m(t) = \alpha T_h(t) + T_{m.a}(t) \tag{17}$$

(17) indicates that the approximate total desired motor torque of MDPS system.

C. ASSISTANT TORQUE OF MOTOR FOR CROSSWIND EFFECT

Here, we investigated the approximate range of additional torque $T_{m.a}(t)$ according to the intensity of ϕ_{cw}. Revisiting to (1) and (14), we have,

$$\dot{v} = a_{11}v + a_{12}r + b_1\delta_f + \phi_{cw} \tag{18}$$

$$\ddot{\delta_f} = -\frac{C_s}{I_s}\dot{\delta_f} - \frac{2\xi K_f}{I_s}\delta_f + \frac{2\xi K_f}{I_s V}v + \frac{2\xi K_f l_f}{I_s V}r + \frac{N_m}{I_s}T_{m.a} + \frac{N_t}{I_s}T_h \tag{19}$$

Applying $\dot{v} \to 0, \ddot{\delta_f} \to 0, \dot{\delta_f} \to 0$ to both (18) and (19), the steady-state responses are given by,

$$a_{11}v_{ss} + a_{12}r_{ss} + b_1\delta_{f.ss} + \phi_{cw.ss} = 0 \tag{20}$$

$$-\frac{2\xi K_f}{I_s}\delta_{f.ss} + \frac{2\xi K_f}{I_s V}v_{ss} + \frac{2\xi K_f l_f}{I_s V}r_{ss} + \frac{N_m}{I_s}T_{m.a.ss} = 0 \tag{21}$$

The above sub-notation ss represents the steady-state condition of each variable in both (18) and (19).

For the given steady-state of crosswind effect $\phi_{cw.ss}$, the steady-state torque $T_{m.a.ss}$, guaranteeing that $v_{ss} \approx r_{ss} \approx 0$, is determined by combining (20) with (21),

$$T_{m.a.ss} = \begin{cases} -\dfrac{\xi m}{N_m}\phi_{cw.ss} & if\ T_{h.ss} = 0 \\ -\dfrac{\xi m}{N_m}\phi_{cw.ss} - \dfrac{N_t}{N_m}T_{h.ss} & if\ T_{h.ss} \neq 0 \end{cases} \tag{22}$$

The first equation in (22) represents the consumption of $T_{m.a}$ for the case without human intervention while the second one in (22) indicates $T_{m.a}$ for the case with human intervention. In addition, it is physically interpreted that if $\phi_{cw.ss} > 0$ and then $T_{h.ss} < 0$ and if $\phi_{cw.ss} < 0$ and then $T_{h.ss} > 0$ because the human reaction $T_{h.ss}$ is exactly opposite to the direction of crosswind effect $\phi_{cw.ss}$. Therefore, the consumption of $T_{m.a.ss}$ in the first equation is greater than the second's, as long as $\phi_{cw.ss} \neq 0$ and $T_{h.ss} \neq 0$. Given the parameter values in **Table 1** and **Table 2**, Fig. 6 describes the results of first equation $T_{m.a.ss}$ in (22) according to the different level of $\phi_{cw.ss}$. Therefore, it can be seen from Fig. 6 that the steady-state torque $T_{m.a.ss}$ requires 4 Nm for an increase of 0.1 $\mathrm{m/s^2}$ corresponding to the aerodynamic force 275 N. Furthermore, the steady-state control power consumption of motor in MDPS system for $\phi_{cw.ss}$ can be roughly determined by the results of Fig. 6. The motor of R-MDPS should adopt this level of torque.

V. CROSSWIND DISTURBANCE COMPENSATION CONTROL STRATEGY

In this section, the design of lateral disturbance control law is presented. According to the requirements in **Section.II**, the control approach considering two cases was discussed: the first case when a driver intervenes steering against the

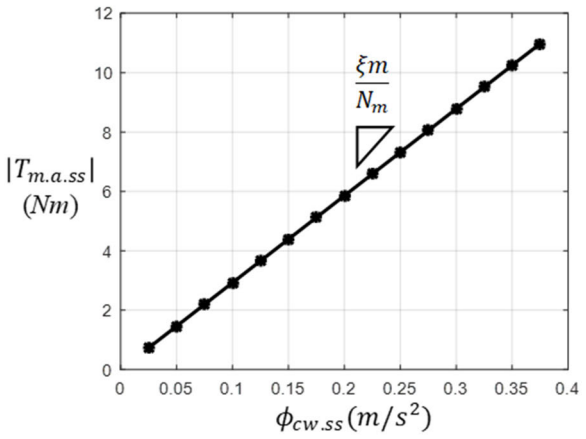

FIGURE 6. Steady-state torque $T_{m.a.ss}$ for $T_{h.ss} = 0$ according to given $\phi_{cw.ss}$.

crosswind effect, and the second case with sudden strong effects of crosswinds causing the driver to temporarily lose steering control. Here, we obtained two different state-space models describing each situation and then applied the optimal control theory to each model. Finally, two different optimal controllers are proposed.

A. CONTROL STRATEGY WITH DRIVER'S INTERVENTION (CONTROL MODE I)

To obtain the first control system, the state-space model describing this case has been derived and the corresponding optimal controller rejecting the disturbance has been designed.

<State-space model for Control mode I>

Substituting (15) through (17) into (14) yields,

$$\ddot{\delta}_f = -\frac{C_s}{I_s}\dot{\delta}_f - \frac{\left(2\xi K_f + K_t N_t N_{tm}\right)}{I_s}\delta_f + \frac{2\xi k_f}{I_s}\left(\frac{v}{V} + \frac{l_f}{V}r\right) + \frac{N_m}{I_s}T_{m.a} + \frac{N_{tm}K_t}{I_s}\theta \quad (23)$$

where, $N_{tm} = [\alpha N_m + N_t] \in \mathbb{R}$. Here, (23) indicates that the front steering angle δ_f is determined by the pure additional torque $T_{m.a}$ and steering wheel angle θ (delivered by a driver).

Combining both (1) and (2) with (23), we have the following state-space model with the state $\boldsymbol{X} = \left[\dot{\delta}_f \;\; \delta_f \;\; v \;\; r\right]^{\boldsymbol{T}} \in \mathbb{R}^{4\times 1}$,

$$\dot{X} = \boldsymbol{A}\boldsymbol{X} + \boldsymbol{B}T_{m.a} + \boldsymbol{E}\boldsymbol{d}$$

$$\begin{bmatrix} \ddot{\delta}_f \\ \dot{\delta}_f \\ \dot{v} \\ \dot{r} \end{bmatrix} = \begin{bmatrix} -\frac{C_s}{I_s} & -\frac{\left(2\xi K_f + K_t N_t N_{tm}\right)}{I_s} & \frac{2\xi K_f}{I_s V} & \frac{2\xi K_f l_f}{I_s V} \\ 1 & 0 & 0 & 0 \\ 0 & b_1 & a_{11} & a_{12} \\ 0 & b_2 & a_{21} & a_{22} \end{bmatrix} \times \begin{bmatrix} \dot{\delta}_f \\ \delta_f \\ v \\ r \end{bmatrix} + \begin{bmatrix} \frac{N_m}{I_s} \\ 0 \\ 0 \\ 0 \end{bmatrix} T_{m.a} + \begin{bmatrix} \frac{N_{tm}K_t}{I_s} & 0 \\ 0 & 0 \\ 0 & 1 \\ 0 & 0 \end{bmatrix} \begin{bmatrix} \theta \\ \phi_{cw} \end{bmatrix} \quad (24)$$

Here, the steering wheel angle θ is embedded into the disturbance vector $\boldsymbol{d} \in \mathbb{R}^{2\times 1}$ in (24), which indicates driver's steering intention. The lateral compensation control strategy for this case should adopt and deal with both the intervention θ and the crosswind effect, ϕ_{cw}.

<Design of controller for mode I>

This section describes the design of controller for the state-space model in (24). **Theorem.2** presents the optimal control law composed of state feed-back control and feed-forward one.

Theorem 2: For (24), the optimal control law of $T_{m.a}$ is given in (25). And, the corresponding optimal control gains are specified in (26) and (27).

$$T_{m.a}(t) = T_{m.aff}(t) + T_{m.afb}(t) \quad (25)$$

$$T_{m.aff}(t) = \boldsymbol{K}_{ff}\, d(t) \;\&\; T_{m.afb}(t) = -\boldsymbol{K}_{fb}\boldsymbol{X}(t) \quad (26)$$

$$\begin{cases} \boldsymbol{K}_{fb} = R^{-1}\boldsymbol{B}^{\boldsymbol{T}}\boldsymbol{P}_{\boldsymbol{ss}} \in \mathbb{R}^{1\times 4} \\ \boldsymbol{K}_{ff} = -R^{-1}\boldsymbol{B}^{\boldsymbol{T}}\boldsymbol{\Upsilon}_{\boldsymbol{ss}} \in \mathbb{R}^{1\times 2} \end{cases} \quad (27)$$

where, $\boldsymbol{P}_{\boldsymbol{ss}} > 0 \in \mathbb{R}^{4\times 4}$ and $\boldsymbol{\Upsilon}_{\boldsymbol{ss}}(t) \in \mathbb{R}^{4\times 1}$ are the unknown positive definite matrix and a vector, respectively and determined by Algebraic Riccatti equation (A.R.E) in (33) and auxiliary equation in (35). Here, the control law consists of two parts, the feed-forward control, $T_{m.aff}(t)$, as counter action for the disturbance d and the state feed-back one, $T_{m.afb}(t)$, for a transient response.

Proof: To find the optimal control law $T_{m.a}$, the Hamiltonian is defined as

$$H(t) = \frac{1}{2}\left(\boldsymbol{X}(\boldsymbol{t})^T\boldsymbol{Q}_{\boldsymbol{c}}\boldsymbol{X}(t) + RT_{m.a}(t)^2\right) + \boldsymbol{\lambda}^T\left(\boldsymbol{A}\boldsymbol{X} + \boldsymbol{B}T_{m.a} + \boldsymbol{E}\boldsymbol{d}\right) \quad (28)$$

where, $\boldsymbol{Q}_{\boldsymbol{c}} > 0 \in \mathbb{R}^{4\times 4}$ and $R > 0 \in \mathbb{R}$ are a positive diagonal definitive matrix and a positive constant. And $\boldsymbol{\lambda} \in \mathbb{R}^{4\times 1}$ is a Largrangian multiplier.

Furthermore, the partial derivative of $H(t)$ with respect to $\boldsymbol{X}(t)$ and $T_{m.a}(t)$ are given by,

$$\frac{\partial H(t)}{\partial \boldsymbol{X}(\boldsymbol{t})} = -\dot{\lambda} \rightarrow -\dot{\lambda} = \boldsymbol{Q}_{\boldsymbol{c}}X(t) + \boldsymbol{A}^{\boldsymbol{T}}\boldsymbol{\lambda} \quad (29)$$

$$\frac{\partial H(t)}{\partial T_{m.a}(t)} = 0 \rightarrow T_{m.a}(t) = -R^{-1}\boldsymbol{B}^T\boldsymbol{\lambda} \quad (30)$$

Assuming $\boldsymbol{\lambda}(t) = \boldsymbol{P}(t)\boldsymbol{X}(t) + \boldsymbol{\Upsilon}(t)$ ($\boldsymbol{P}(t) > 0 \in \mathbb{R}^{4\times 4}$and $\boldsymbol{\Upsilon}(t) \in \mathbb{R}^{4\times 1}$ are the unknown positive definite matrix and vector, respectively) and taking the derivative of $\boldsymbol{\lambda}(t)$ with respect of a time yields,

$$\dot{\lambda} = \dot{\boldsymbol{P}}(t)\boldsymbol{X}(t) + \boldsymbol{P}(t)\dot{X}(t) + \dot{\Upsilon}(t) \quad (31)$$

Combining (24), (29), (30) with (31) yields,

$$\left(\dot{P} + \boldsymbol{PA} - \boldsymbol{PBR}^{-1}\boldsymbol{B}^{T}\boldsymbol{P} + \boldsymbol{Q_c} + \boldsymbol{A}^{T}\boldsymbol{P}\right)\boldsymbol{X}(t) + \left[\dot{\Upsilon}(t) + \left(\boldsymbol{A}^{T} - \boldsymbol{PB}\,R^{-1}\boldsymbol{B}^{T}\right)\boldsymbol{\Upsilon}(t) + \boldsymbol{PEd}\right] = \boldsymbol{0} \tag{32}$$

Allowing $\dot{P} \rightarrow \boldsymbol{0}$ for the steady-state condition (denoted as $\boldsymbol{P_{ss}}$) of $\boldsymbol{P}$,and then the above equation (32) generate an A.R.E and an auxiliary one,

$$\boldsymbol{P_{ss}}\,\boldsymbol{A} - \boldsymbol{P_{ss}}\boldsymbol{BR}^{-1}\boldsymbol{B}^{T}\boldsymbol{P_{ss}} + \boldsymbol{Q_c} + \boldsymbol{A}^{T}\boldsymbol{P_{ss}} = 0 \tag{33}$$

$$\dot{\Upsilon}(t) + \left(\boldsymbol{A}^{T} - \boldsymbol{P_{ss}}\boldsymbol{BR}^{-1}\boldsymbol{B}^{T}\right)\boldsymbol{\Upsilon}(t) + \boldsymbol{P_{ss}}\boldsymbol{Ed} = 0 \tag{34}$$

It is well known that the solution of (33) exist and well-defined. And, the steady-state solution of $\boldsymbol{\Upsilon}(t)$ can be possibly obtained by allowing $\dot{\Upsilon}(t) \rightarrow \boldsymbol{0}$ since d is assumed as time-varying excitation with finite slopes. Hence, based on (34), we have,

$$\boldsymbol{\Upsilon_{ss}}(t) = -\left(\boldsymbol{A}^{T} - \boldsymbol{PBR}^{-1}\boldsymbol{B}^{T}\right)^{-1}\boldsymbol{PEd} \tag{35}$$

Therefore, based on (30), (33) and (35), the final control law is determined as shown in (25). The proof completed ■.

<Control gain selection for the control mode I>

To choose the proper gains, $\boldsymbol{K_{fb}}$ and $\boldsymbol{K_{ff}}$, in (26) and (27), the characteristic equation and frequency responses of the closed-loop system is investigated for the different $\boldsymbol{Q_c}$ and a fixed R in (28). Specifically, $\boldsymbol{Q_c} = q_c\,\mathbf{diag}\left[\,0.5\;\;1\;\;5\;\;5\,\right]$ and $R = 0.1$ are selected and, based on the variation of q_c in $\boldsymbol{Q_c}$, the trajectory of roots of the closed-loop system together with the poles of open-loop system (i.e, $\boldsymbol{s_i}$ for $\boldsymbol{i} = 1, 2, 3, 4$ $\boldsymbol{of}$ $|\boldsymbol{sI} - \boldsymbol{A}| = \boldsymbol{0}$) is described in Fig. 7(a) while the corresponding gains $\boldsymbol{K_{ff}} = \left[K_{ff.1}K_{ff.2}\right]$ of feed-forward control are specified in Fig. 7(b). As seen from (34), the feed-forward gain K_{ff} includes the matrix $\boldsymbol{P_{ss}}$ which is function of $\boldsymbol{Q_c}$. As norm of $\boldsymbol{Q_c}$, $\left\|\boldsymbol{Q_c}\right\|$, increases, K_{ff} does. It should be mentioned that the open-loop system is already stable (all poles of open-loop system $\boldsymbol{s_i}$ lie on the left-half Re-Im plane as seen from Fig. 7(a)) since we introduced (15) to (14) (i.e, a driver included). Also, Fig. 7(c) represents three frequency responses for the cases $q_c = 0.01$, $q_c = 2$, and $q_c = 17.8$, where we can see more gain margins as q_c increases. Based on the results of Fig. 7(a),(b), and (c), to minimize the 2nd order characteristic transient and avoid an excessive feed-forward effort, the case with $q_c = 2$ is used for the proposed control system.

B. CONTROL STRATEGY WITHOUT DRIVER'S INTERVENTION (CONTROL MODE)

Similarly, to obtain the second control system, the state-space model describing this situation has been presented here and the corresponding optimal controller has been designed using same technique in **Theorem.2**.

<State-space model for the control mode II>

If there is no human intervention, it is clear that $T_h(t) \approx 0$. For this case, based on (1) and (2) with (14), the following state-space model can be obtained,

$$\dot{X} = \boldsymbol{A_{w/o}}\boldsymbol{X} + \boldsymbol{Bu} + \boldsymbol{E_{w/o}}\phi_{cw}$$

$$\begin{bmatrix} \ddot{\delta}_f \\ \dot{\delta}_f \\ \dot{v} \\ \dot{r} \end{bmatrix} = \begin{bmatrix} -\frac{C_s}{I_s} & -\frac{2\xi K_f}{I_s} & \frac{2\xi K_f}{I_s V} & \frac{2\xi K_f l_f}{I_s V} \\ 1 & 0 & 0 & 0 \\ 0 & b_1 & a_{11} & a_{12} \\ 0 & b_2 & a_{21} & a_{22} \end{bmatrix} \begin{bmatrix} \dot{\delta}_f \\ \delta_f \\ v \\ r \end{bmatrix} + \begin{bmatrix} \frac{N_m}{I_s} \\ 0 \\ 0 \\ 0 \end{bmatrix} T_{m.a} + \begin{bmatrix} 0 \\ 0 \\ 1 \\ 0 \end{bmatrix} \phi_{cw} \tag{36}$$

Now, compared to (24), we have different matrix $\boldsymbol{A_{w/o}} \in \mathbb{R}^{4\times4}$ and vector $\boldsymbol{E_{w/o}} \in \mathbb{R}^{4\times1}$ adopting the situation where no driver is involved. Especially, one disturbance, ϕ_{cw} appears in (36).

<Design of controller for mode II>

The feed-forward term, $\boldsymbol{\Upsilon}_{ss}(t) \in \mathbb{R}^{4\times1}$, is determined by,

$$\boldsymbol{\Upsilon_{ss}}(t) = -\left(\boldsymbol{A}_{\boldsymbol{w/o}}^{T} - \boldsymbol{P_{w/o.ss}}\boldsymbol{BR}^{-1}\boldsymbol{B}^{T}\right)^{-1}\boldsymbol{P_{w/o.ss}}\boldsymbol{E_{w/o}}\phi_{cw} \tag{37}$$

where $\boldsymbol{P_{w/o.ss}} > 0 \in \mathbb{R}^{4\times4}$ is the positive definitive matrix obtained by A.R.E based on $\boldsymbol{A_{w/o}}$,as shown in (38),

$$\boldsymbol{P_{w/o.ss}}\boldsymbol{A_{w/o}} - \boldsymbol{P_{w/o.ss}}\boldsymbol{BR}^{-1}\boldsymbol{B}^{T}\boldsymbol{P_{w/o.ss}} + \boldsymbol{Q} + \boldsymbol{A}_{\boldsymbol{w/o}}^{T}\boldsymbol{P_{w/o.ss}} = 0 \tag{38}$$

Therefore, the final control law of $T_{m.a}$ for the case without a driver input is determined by,

$$\begin{aligned} T_{m.a}(t) &= T_{m.a.ff}(t) + T_{m.a.fb}(t) \\ &= -\boldsymbol{K_{fb}}\boldsymbol{X}(t) + K_{ff}\phi_{cw}(t) \end{aligned} \tag{39}$$

where, $\boldsymbol{K_{fb}} = R^{-1}\boldsymbol{B}^{T}\boldsymbol{P_{w/o.ss}} \in \mathbb{R}^{1\times4}$ and $K_{ff} = -R^{-1}\boldsymbol{B}^{T}\boldsymbol{\Upsilon}_{ss}(t) \in \mathbb{R}$.

<Control gain selection for control mode II>

Also, to obtain the proper, $\boldsymbol{K_{fb}}$ and K_{ff}, in (39), the characteristic equation of the closed-loop system is explored according to the different $\boldsymbol{Q_c}$. Similarly, $\boldsymbol{Q_c} = q_c\,\mathbf{diag}\left[\,0.5\;\;1\;\;5\;\;5\,\right]$ and $R = 0.1$ are selected and, based on the variation of q_c in $\boldsymbol{Q_c}$, the trajectory of roots of the closed-loop system together with the poles of open-loop system (i.e, $s_i$for$i = 1, 2, 3, 4$of$\left|s\,\boldsymbol{I} - \boldsymbol{A_{w/o}}\right| = \boldsymbol{0}$) is described in Fig. 8(a). And, the corresponding gain K_{ff} of feed-forward control is presented in Fig. 8(b). Compared to the previous situation in Fig. 7(a), Fig. 8(a) indicates that the open-loop system is unstable. Fig. 8(c) represents three frequency responses for the cases $q_c = 0.01$, $q_c = 2$, as well as $q_c = 17.8$, where we can see more gain margins as q_c increases. Based on the results of Fig. 8(a),(b), and (c), to minimize the 2nd order characteristic transient and a feed-forward effort, $q_c = 2$ is chosen for the proposed control system. This leads that the vehicle is smoothly controlled by the control system, allowing a driver to firmly re-grip a steering wheel.

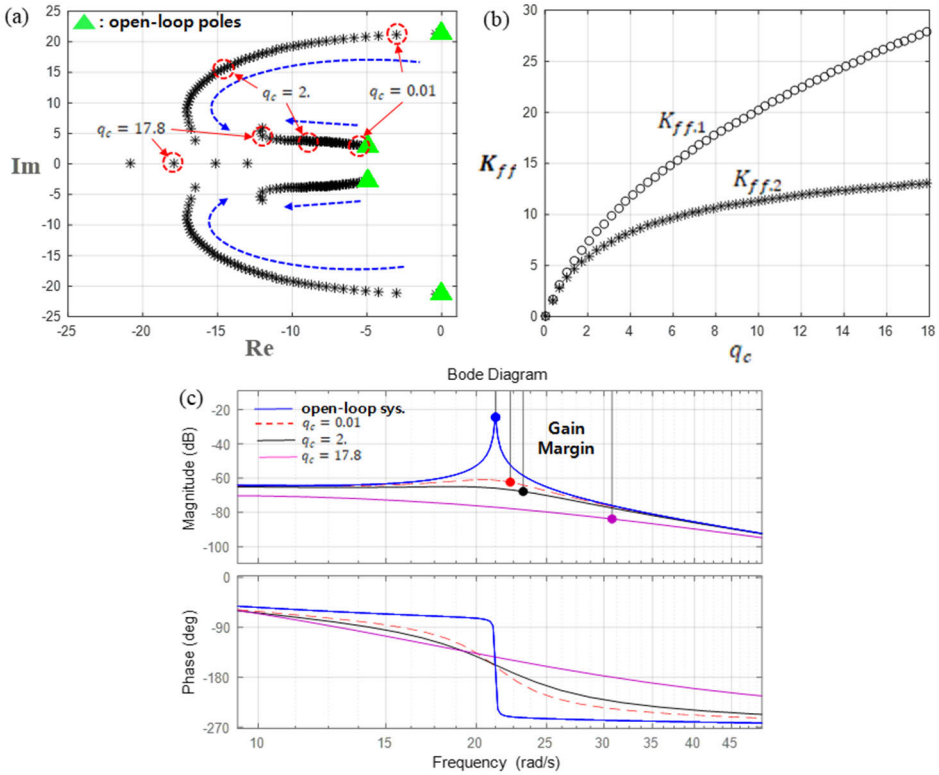

FIGURE 7. Trajectory of roots for the closed-loop system and the corresponding feed-forward control gains for the case with diver intervention: (a) Trajectory of roots for the closed-loop system (b) Corresponding gains of feed-forward control and (c) Corresponding frequency responses.

C. DETECTION CONDITION AND CONTROL MODE SELECTION STRATEGY

In order to achieve desired and efficient operation of the two designed control system (shown in the previous subsections), it is very important to address the critical intensity of the estimated crosswind and the appropriate selection criteria for each control mode. Therefore, in this subsection, the detection conditions for the crosswind effect and the control mode selection strategy between the two controls were thoroughly discussed.

<Primary detection criterion of crosswind >

To suggest the primary criterion that the crosswind intensity is sufficiently and constantly effective to disturb a driver or the status of the vehicle, we considered the steady-state dynamic response of the vehicle in the absence of driver's intervention for the different level of crosswind. The reason why the case of no driver intervention should be considered is that the pure dynamic state of the vehicle is important in the absence of an assistance system or human driver control after crosswind is impacted to the vehicle. In other words, such pure condition will provide a clear judgment as to whether a particular crosswind is effective or not. In the absence of lateral disturbance compensation and driver intervention, (36) becomes,

$$\dot{X} = \boldsymbol{A_{w/o}} \boldsymbol{X} + \boldsymbol{E_{w/o}} \phi_{cw} \tag{40}$$

The above equation (40) indicates the pure dynamic response of vehicle system for a given the crosswind effect ϕ_{cw}.

The transfer function of (40) for the input ϕ_{cw} is given by,

$$\boldsymbol{X}(s) = \left(s\boldsymbol{I} - \boldsymbol{A_{w/o}}\right)^{-1} \boldsymbol{E_{w/o}} \phi_{cw}(s) \tag{41}$$

Especially, focusing on the transfer function about the yaw rate $r(s)$ for $\phi_{cw}(s)$,

$$r(s) = \boldsymbol{C}_r \boldsymbol{X}(s) = \boldsymbol{C}_r \left(s\boldsymbol{I} - \boldsymbol{A_{w/o}}\right)^{-1} \boldsymbol{E_{w/o}} \phi_{cw}(s) \tag{42}$$

where, $\boldsymbol{C}_r = \begin{bmatrix} 0 & 0 & 0 & 1 \end{bmatrix} \in \mathbb{R}^{1\times 4}$ is an adopting vector to select the response, r(s).

Assuming that a crosswind is described as a step-like input, the steady-state response of $r(s)$ to the step input $\phi_{cw}(s) = \phi_{cw.ss}/s$ is given via the final value theorem as followed,

$$r_{ss} = \lim_{s\to 0} \boldsymbol{C}_r \left(s\boldsymbol{I} - \boldsymbol{A_{w/o}}\right)^{-1} \boldsymbol{E_{w/o}} \phi_{cw.ss} \tag{43}$$

where, r_{ss} is the steady-state response of $r(t)$ and $\phi_{cw.ss} \in \mathbb{R}$ is a constant representing the intensity of crosswind.

Based on (43), the responses of r_{ss} for the different levels of both $\phi_{cw.ss}$ and the longitudinal velocity V are described in Fig. 9(a). In other words, the results of Fig. 9(a) represent the distribution $r_{ss} = f(\phi_{cw.o}, V)$, which indicates how the vehicle's direction is changed by the crosswind effect.

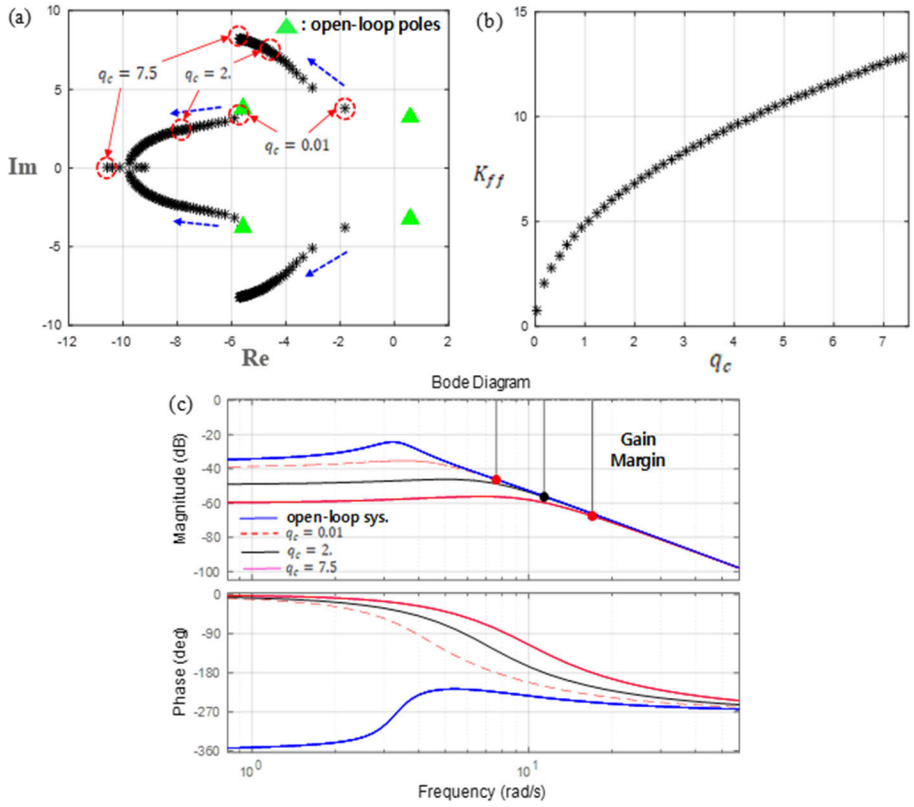

FIGURE 8. Trajectory of Roots for the closed-loop system and the corresponding gains of feed-forward control for the case without a diver input: (a) Trajectory of Roots for the closed-loop system (b) Corresponding gains of feed-forward control (c) Frequency responses.

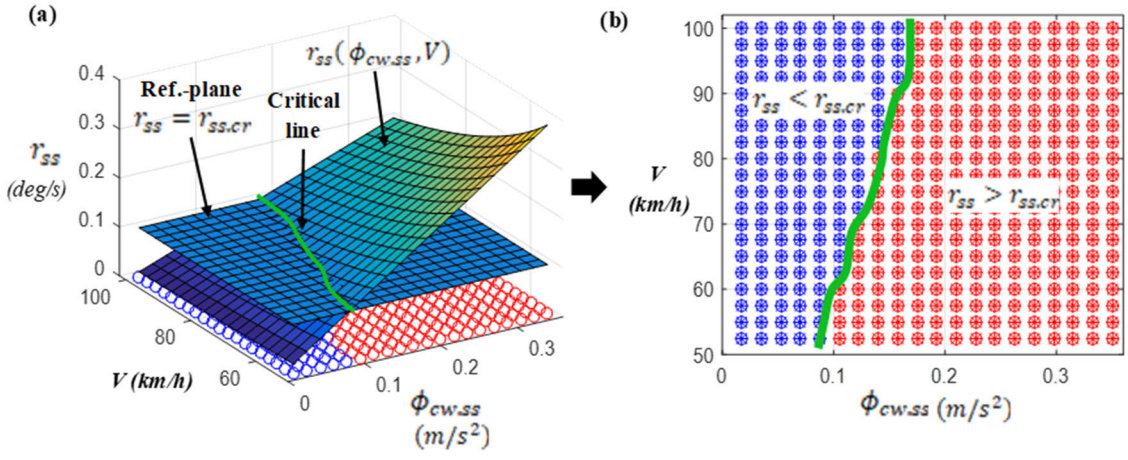

FIGURE 9. Steady-state responses of yaw rate r(t) for $\phi_{cw.ss}$ and the longitudinal velocity V (a) $\mathbb{R}_{ss}$ for $\phi_{cw.ss}$ and V and (b) $\phi_{cw.ss}$ and V on the projected plane.

It can be seen from Fig. 9(a) that r_{ss} increases as $\phi_{cw.ss}$ become stronger. However, this effect diminishes at higher V due to the stronger inertial force of the vehicle. Therefore, by choosing the critical steady-state value of the yaw rate, the results in Fig. 9(a) allow us to define a critical condition of $\phi_{cw.ss}$ such as whether the crosswind sufficiently affects the vehicle.

This leads that, selecting $r_{ss.cr}$, we have,

$$r_{ss}\left(\phi^*_{cw.o}, V^*\right) = r_{ss.cr} \tag{44}$$

where, $\phi^*_{cw.o}$ and V^* are the corresponding critical crosswinds and velocities for the $r_{ss.cr}$, which implies that the vehicle is not critically subject to crosswind below $\phi^*_{cw.o}$. Both $\phi^*_{cw.o}$ and V^* are specified by the terms of ''critical line'' in

Fig. 9(a) and (b). Here, $r_{ss.cr}$ is selected as 0.1 deg/s for this study.

Based on (44), the detection condition of effective crosswind in the aspect of r_{ss} is given by,

$$\phi_{cw} > \phi_{cw.o}{}^{*} \tag{45}$$

As seen from the critical line in Fig. 9(b), $\phi_{cw.o}{}^{*}$ slightly varies according to the different V. Thus, we can establish the specific detection condition of effective crosswind for V based on Fig. 9 and the corresponding $\phi_{cw.o}{}^{*}$ is approximately given by,

$$\phi_{cw.o}{}^{*} = \begin{cases} 0.1 \; if \; 50 < V < 70 \left(km/h\right) \\ 0.13 \; if \; 70 \le V < 80 \left(km/h\right) \\ 0.16 \; if \; V \ge 80 \left(km/h\right) \end{cases} \tag{46}$$

<Control mode selection condition >

Next, in addition to the primary detection condition in (46), we need to find the selection condition of control mode to activate either the first control mode C_1 (shown in (25)) or the second control one C_2 (shown in (39)). For this purpose, two indicators are proposed: a steering wheel torque $T_h(t)$ and a yaw rate $r(t)$. The reason for choosing these two is based on the fact that $T_h(t)$ and $r(t)$ represent the driver's effort and vehicle state that must be manipulated by the proposed control system. The lateral velocity $v(t)$ is also an important state that describes the vehicle state, but is usually proportional to $r(t)$. Therefore, only $r(t)$ was chosen to construct the selection condition. Also, it should be emphasized that this selection condition is capable of constraining the control torque of motor and steering wheel torque. This point of view will be elaborated in **Section VI**.

Remarks 2 (Case With Driver Intervention and First Control Mode C_1): when challenging a sudden step-like crosswind, the driver holds the steering wheel firmly and counter-steer to avoid allowing the vehicle to deviate from its original desired travel path (i.e, a straight road). As a result, the steering wheel torque $T_h(t)$ transmitted by the driver increases while the steady-state value of the yaw rate remains negligible by the effort of the driver (although there exists a considerable transient of r(t) including high peak). However, $T_h(t)$ will be decreased after the first compensation control (C_1) in (25), designed to reduce a steering effort, is initiated.

Remarks 3 (Case Without Driver Intervention and Second Control Mode C_2): For an identical crosswind situation, if the driver fails to adequately respond to the crosswind effect and loses the steering control, it is clear that $T_h(t)$ is relatively small to the case in **Remarks. 2** but the yaw rate $r(t)$ of the vehicle increases due to the crosswind effect. As a result, the car deviates from the desired trajectory. However, $T_h(t)$ will be increased eventually if the second compensation control (C_2) in (39) is activated because the motor/actuator tries to overcome the crosswind effect and then generate the counter-steer by inducing the opposite non-zero front steering angle. This implies that $T_h(t)$ is not made by a driver but is created by the control system. This point of view for **Remarks. 2** and **3** will be discussed along with the simulation results in next **Section**.

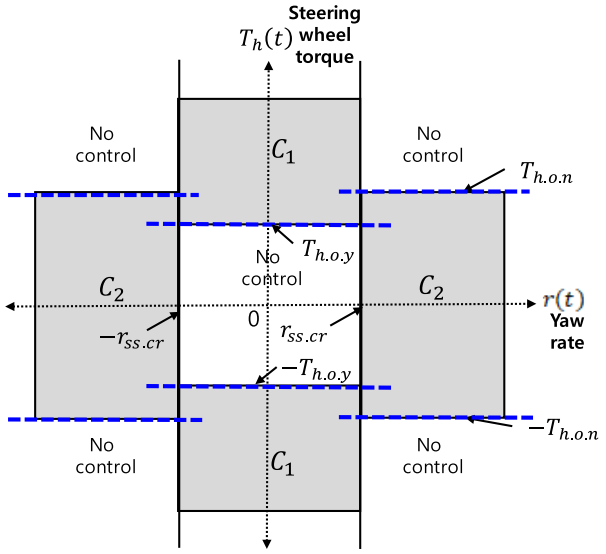

FIGURE 10. Control mode selection conditions specified on the plane of yaw rate r(t) and steering wheel torque $T_h(t)$.

Furthermore, considering both **Remarks. 2** and**3** above, the condition whether the driver intervenes steering or not under the situation $\phi_{cw.o}{}^{*}$ and, simultaneously, whether the control system select C_1 or C_2 are imposed by,

$$if \; \phi_{cw} > \phi_{cw.o}{}^{*} \rightarrow \begin{cases} C_1 \rightarrow if \;\; |T_h(t)| > T_{h.o.y} \& \, |r(t)| < r_{ss.cr} \\ C_2 \rightarrow if \;\; |T_h(t)| < T_{h.o.n} \& \, |r(t)| > r_{ss.cr} \\ No \; Control \quad otherwise \end{cases} \tag{47}$$

where, C_1 and C_2 indicate the first control mode and the second control one, respectively. And, $T_{h.o.y}$ and $T_{h.o.n}$ (i.e, not made by a driver) represents the threshold torques indicating the minimum steering effort for C_1 and the maximum steering effort for C_2. The condition "No control" in (47) indicates a situation in which a driver uses minimum steering effort or intends to steer the vehicle to another lane, even if affected by a crosswind. The condition (47) is visualized on the plane of yaw rate $r(t)$ and steering wheel torque $T_h(t)$ (i.e, $r(t)$ vs.$T_h(t)$), as shown in Fig. 10.

Remarks 4 (Averaging of Control Torque at the Boundary of Control Mode Selection): The minimum threshold torque $T_{h.o.y}$ in C_1 determines the final steady-state of the steering wheel torque as $T_{h.o.y}$ as long as the control is active. On the other hand, the maximum torque $T_{h.o.n}$ in C_2 induces a state in which $T_h(t)$ reaches $T_{h.o.n}$ under the control. In other words, $\lim_{t\to\infty} T_h(t) \rightarrow T_{h.o.y}$ via C_1 and $\lim_{t\to\infty} T_h(t) \rightarrow T_{h.o.n}$ via C_2. For this purpose, however, this control strategy generates an on-and-off in control torque signal at the boundaries of the control selection condition (in Fig. 10), as described in Fig. 11 (b) and (c). Therefore, the averaging signal conditioning for the control torque is required and can be performed via a proper low-pass filter as shown in Fig. 11(a).

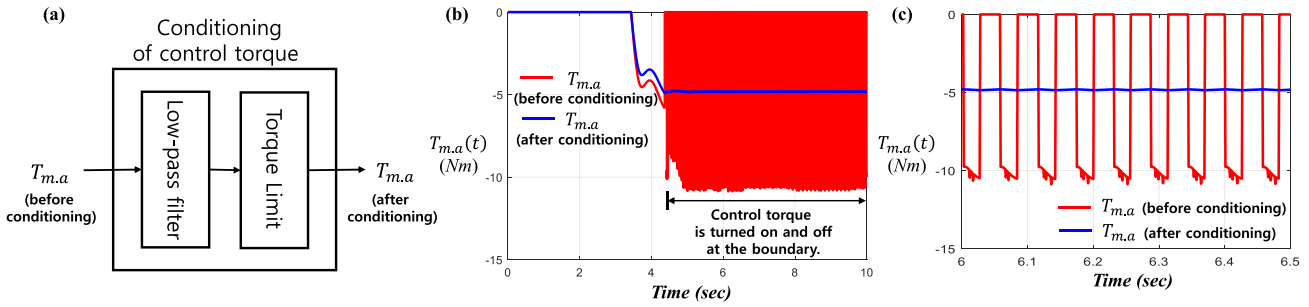

FIGURE 11. Averaging of control torque at the boundary: (a) Conditioning process of desired torque, (b) Simulation results of averaging torque at boundary, and (c) Zoom of (b) in the range from 6 to 6.5 secs.

In addition, the entire control flow of lateral compensation strategy together with both the detection condition (46) and the control mode selection condition (47) is described in Fig. 12.

Specifically, it can be seen from Fig. 12 that the controller receives $\widehat{\boldsymbol{X}}_e$ from the observer and the front steering angle δ_f from the vehicle/steering system, while the vehicle sends $\boldsymbol{y}_e$ to the observer. Finally, the controller commands the steering system the demanded assistance torque $T_{m.a}$ (after conditioning) after averaging the torque $T_{m.a}$ (before conditioning) through the conditioning process.

VI. PERFORMANCE EVALUATION OF LATERAL DISTURBANCE CONTROL SYSTEM

In this section, we evaluated the proposed lateral disturbance compensation strategy using several crosswind scenarios in Carsim/Simulink co-simulation and HILS environments. Fig. 13 shows the estimation and control performances for the case with human driver intervention under the influence of step-like crosswind effect. Here, to include a human driver in this simulation process, we used a human driver model with a preview time 0.22 (sec) provided by Carsim. Fig. 13(a) presented the estimates of $\phi_{cw}(t)$ which well tracks the true effect (described as the dotted line). Fig. 13(b) and (c) describe the yaw rate of vehicle $r\,(t)$ and the lateral acceleration of vehicle $a_y\left(m/s^2\right)$ on the time-domain. And Fig. 13(d) and (f) represent the assistance torque of motor $T_{m.a}\,(t)$ and the steering wheel torque $T_h\,(t)$ consumed by a driver. Here, the mode selection variables are chosen as $T_{h.o.y} = T_{h.o.n} = 1\,(Nm)$ and $r_{ss.cr} = 0.1\left(deg/s\right)$. Fig. 13(f) indicates the trajectory of vehicle ($x(m)$ vs. $y(m)$). According to Fig. 13(b), (c), and (f), it is found that the vehicle motions between the case with control and the one without control are almost identical due to the human driver's intervention. This implies that the control assistance does not perturb the entire motion of vehicle significantly, causing less discomfort to the driver. However, it is clear from Fig. 13(e) that the steering effort (i.e, torque) via a driver has been three-time reduced by the proposed lateral disturbance control compared to the case without the control and finally reaches 1 Nm due to $T_{h.o.y} = 1Nm$ (i.e, $\lim_{t\to\infty} T_h\,(t) \to T_{h.o.y}$ according to **Remarks. 4**). This reduction can be fortified if we choose another $T_{h.o.y}$ less than 1 Nm. Together with **Remarks. 2**, this point of view will be discussed in Fig. 15. On the other hands, Fig.14 shows the estimation and control performances for the case where a driver lost a steering control due to the influence of step-like crosswind effect. Here, to exclude a human driver for the simulation process, we disabled the driver model in Carsim. Fig. 14(a) presented the estimates of $\phi_{cw}(t)$ and it can be seen that the estimate is well synchronized with the assumed actual crosswind effect. Fig. 14(b) and (c) describe the yaw rate of vehicle $r\,(t)$ and the lateral acceleration of vehicle $a_y(t)$. And, Fig. 14(d) and (f) represent the assistance torque of motor $T_{m.a}\,(t)$ and the steering wheel torque $T_h\,(t)$. Here, the control mode selection variables $T_{h.o.n} = T_{h.o.y} = 1\,(Nm)$ and $r_{ss.cr} = 0.1\left(deg/s\right)$ are used. Fig. 14(f) indicates the trajectory of vehicle ($x(m)$ vs. $y(m)$). According to Fig. 14(b), (c), and (f), it is found that the vehicle motions between the case with control and the one without control are significantly different due to the action of lateral disturbance control. Since the case in Fig. 14 describes the situation for no human driver intervention, the control system completely overrides entire steering process to decrease the unexpected crosswind effect on the vehicle. Consequently, the heading angle change (i.e, yaw rate) and the lateral speed (i.e, $v(t)$) of the vehicle have been reduced by almost 40%. We can see this point of view from the vehicle trajectory shown in Fig. 14(f), either. However, the motor torque used for this situation is slightly increased compared to the case in Fig. 13(d). This indicates that the control system is solely responsible for the steering control of vehicle without any assistance from a driver. Furthermore, Fig. 14(e) represents the steering torque produced by control system, instead of a driver, approximately approaches 1 Nm since $T_{h.o.n}$ is chosen as 1 Nm (i.e, $T_h\,(t) \to T_{h.o.n}$ according to **Remarks. 4**). Similarly, controlling the value $T_{h.o.n}$ yields the different performances, which will be explored in Fig. 18. Furthermore, Fig. 15 describes the partial trajectory of $r\,(t)$ and $T_h\,(t)$ in the detection condition for both Fig. 13 and Fig. 14 after the crosswind effect is detected (i.e. $\phi_{cw} > \phi_{cw.o}{}^*$). It is found that the trajectory of $r\,(t)$ and $T_h\,(t)$ for Fig. 13 lies on the region C_1 while the trajectory for Fig. 14 does on the region C_2. The results imply that the control precisely operates according to the control

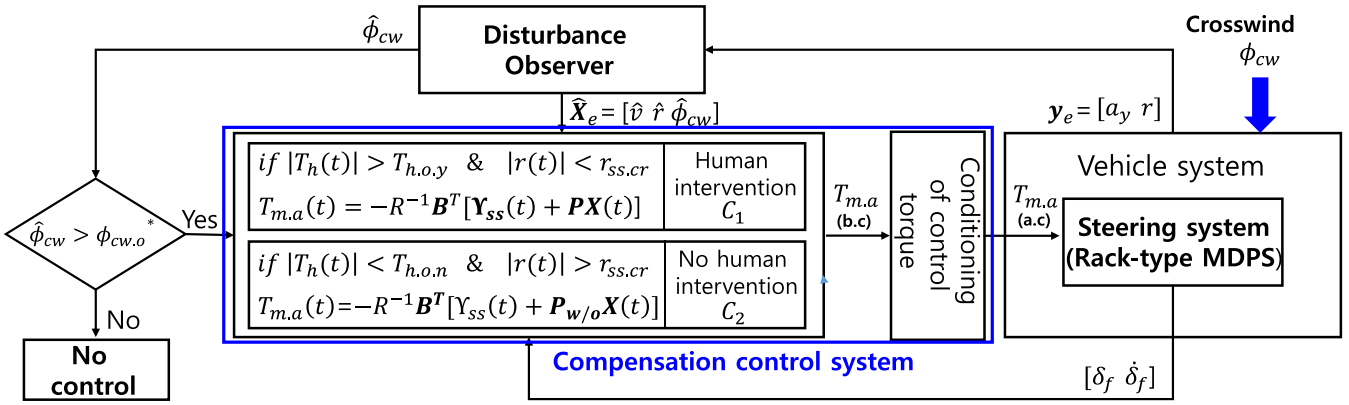

FIGURE 12. Entire control flow of lateral compensation strategy with other major components, an observer and the vehicle system.

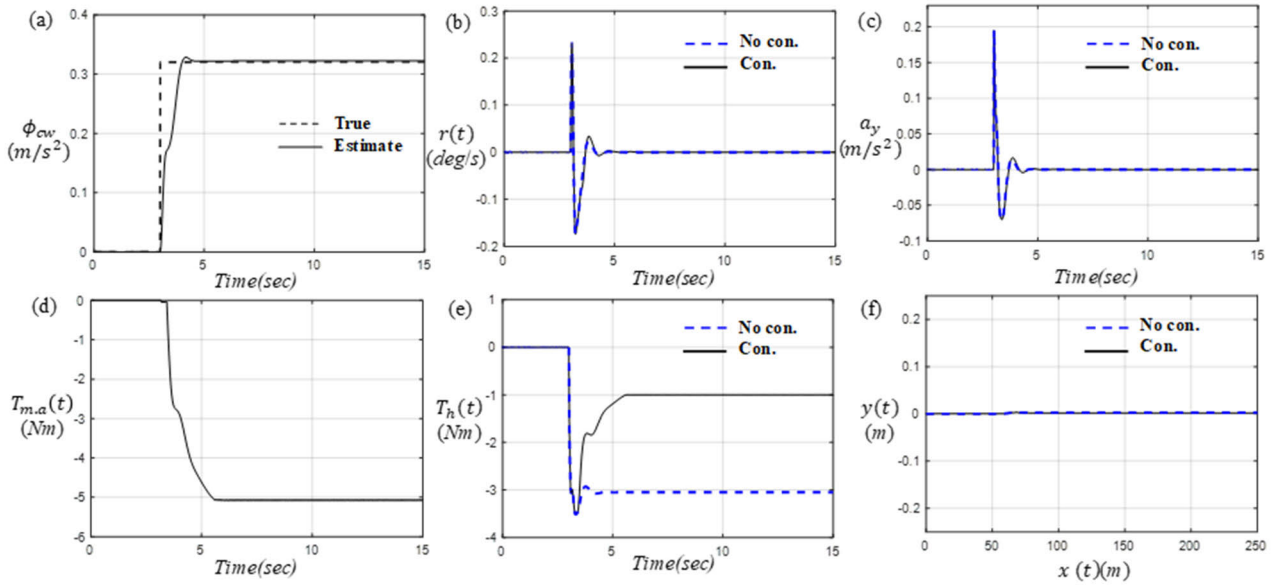

FIGURE 13. Estimation and control performances for the case with human driver intervention under the influence of crosswind effect (a) Estimates of ϕ_{cw}, (b) Yaw rate of vehicle $\mathbb{R}(t)$ (c) Lateral acceleration of vehicle a_y (m/s^2), (d) Assistance torque of motor $T_{m.a}(t)$, (e) Steering wheel torque $T_h(t)$, and (f) The trajectory of vehicle (x(m) vs. y(m)).

mode selection conditions shown in Fig. 10. In addition, Fig. 16 presents the estimation and control performances for the case with human driver intervention under the influence of more complicate crosswind scenario (i.e, no wind, positive direction wind, no wind, negative direction wind, and no wind in an order). Fig. 16(a) indicates the estimates of actual ϕ_{cw} and shows that the directions (positive and negative) and magnitudes of ϕ_{cw} are well estimated via the proposed observer. Fig. 16(b) and (c) describe the yaw rate of vehicle, $r\ (t)$, and the lateral acceleration of vehicle, a_y. And Fig. 16(d) and (f) represent the assistance torque of motor $T_{m.a}\ (t)$ and the corresponding steering wheel torque $T_h\ (t)$. Fig. 16(f) describes the trajectories of $r\ (t)$ and $T_h\ (t)$ on the control mode selection conditions. According to Fig. 16(b) and (c), it is found that, regardless of controls, the vehicle motions are almost identical due to the action of driver, which is synchronized with the results in Fig. 13. Similar to Fig. 13(e), Fig. 16(e) shows that the steering effort (i.e, torque) via a driver has been three-time reduced by the proposed control technique compared to the case with no control. As seen from Fig. 16(f), it is clear that the partial trajectory of $r\ (t)$ and $T_h\ (t)$, after the control is initiated, exactly lies on the region C_1.

Fig. 17 explores the performance of the tuned control system with slight changes to the control mode selection conditions. Fig. 17 describes the consumed torques of both assistance motor and human driver according to the three expanded $\boldsymbol{C_1}$ regions. Here, three different $T_{h.o.y}$, 0.5 Nm, 1.0 Nm and 1.5 Nm are used. This indicates that the target torque of steering wheel (i.e, the final steady-state torque) is changed, causing less steering effort by a driver. Therefore, according to Fig. 17(a) and (b), we can see that the assistance motor torque increases as $T_{h.o.y}$ decreases. This is obvious as

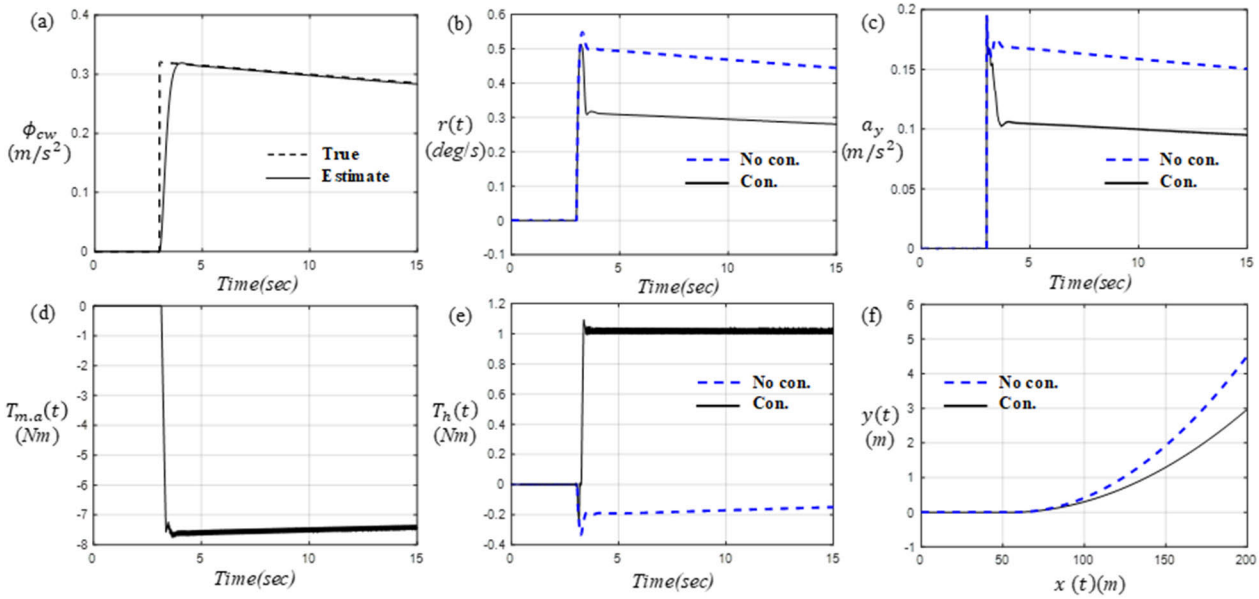

FIGURE 14. Estimation and control performances for the case without human driver intervention under the influence of crosswind effect (a) Estimates of ϕ_{cw}, (b) Yaw rate of vehicle $\mathbb{R}\ (t)$ (c) Lateral acceleration of vehicle $a_y\ (m/s^2)$, (d) Assistance torque of motor $T_{m.a}\ (t)$, (e) Steering wheel torque $T_h\ (t)$, and (f) The trajectory of vehicle (x(m) vs. y(m)).

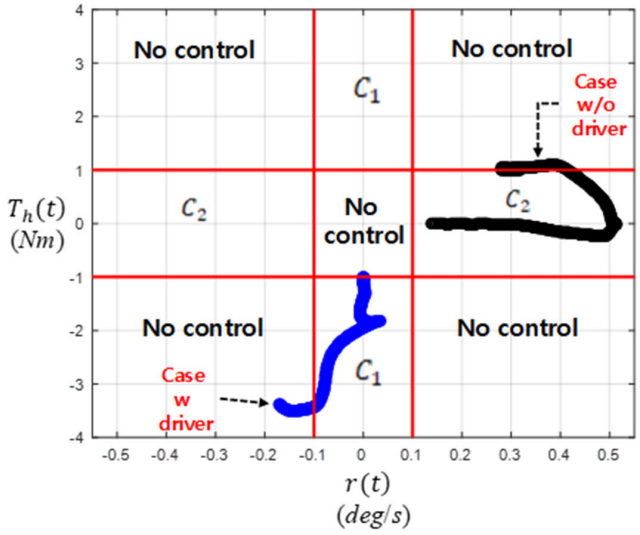

FIGURE 15. The trajectory of $\mathbb{R}\ (t)$ and $T_h\ (t)$ for both the first control mode and the second one on the plane of detection condition ($T_{h.o.y} = 1\ (Nm)$, $T_{h.o.n} = 1\ (Nm)$ and $\mathbb{R}_{ss.cr} = 0.1\ (deg/s)$.

more assist torque is needed to reduce the driver's steering effort in the end. Also, the results of Fig. 17 show that the proposed control method can select the assistance intensity, which is a clear advantage of the control strategy in this study. Also, the final steady-state torques in Fig. 17(b) reach 0.5 Nm, 1.0 Nm and 1.5 Nm, which is exactly matched with Remarks. 4 (i.e, $\boldsymbol{T_h}\ (\boldsymbol{t}) \lim_{t\to\infty} \rightarrow \mathbf{0.5,\ 1.0,1.5}$). Similar to Fig. 17, Fig. 18 presents the control performances for the three expanded C_2 regions (see Fig. 18(d)). By expanding the region C_2 in terms of steering wheel torque $\boldsymbol{T_h}\ (\boldsymbol{t})$, the yaw rate and the lateral deviation of vehicle have been reduced because the control action $\boldsymbol{T_{m.a}}\ (\boldsymbol{t})$ induced a counter-steering $\boldsymbol{\delta_f}\ (\boldsymbol{t})$ even no driver's steering, which eventually increases the difference between $\boldsymbol{\theta}\ (\boldsymbol{t})$ and $\boldsymbol{\delta_f}\ (\boldsymbol{t})$. This leads that $\boldsymbol{T_h}\ (\boldsymbol{t})$ augments as predicted by (15). The motor/actuator tries to overcome the crosswind effect and then generate the counter-steer by inducing the opposite non-zero front steering angle $\boldsymbol{\delta_f}\ (\boldsymbol{t})$ according to the strategy in (39) (i.e, $\boldsymbol{X}\ (\boldsymbol{t})$ in (39) includes $\boldsymbol{\delta_f}\ (\boldsymbol{t})$). However, the steering wheel angle $\boldsymbol{\theta}\ (\boldsymbol{t})$ is not changed much since there is no driver intervention but $\boldsymbol{\delta_f}\ (\boldsymbol{t})$ is relatively changed. In other words, before control, $\boldsymbol{T_h}\ (\boldsymbol{t})$ is small since there is no driver intervention (i.e, $\boldsymbol{\theta}\ (\boldsymbol{t}) \approx \mathbf{0}$ and $\boldsymbol{\delta_f}\ (\boldsymbol{t}) \approx \mathbf{0}$) but $\boldsymbol{T_h}\ (\boldsymbol{t})$ gradually increases after control (i.e, $\left|\boldsymbol{N_t\delta_f}\ (\boldsymbol{t})\right| > |\boldsymbol{\theta}\ (\boldsymbol{t})| \approx \mathbf{0}$). This is the explanation of Remarks.4. To maximize the control performance for the case without driver intervention, the region C_2 should be manipulated as shown in Fig. 18(d). Also, the final steady-state torques in Fig. 18(b) reach $\boldsymbol{T_{h.o.n.1}} = 1.0Nm$, $\boldsymbol{T_{h.o.n.2}} = 1.5Nm$, and $\boldsymbol{T_{h.o.n.3}} = 2.2Nm$, which is exactly synchronized with Remarks.4. Furthermore, we investigated the control performance of proposed control system based on more realistic crosswind effect scenario (shown in Fig. 19 and Fig. 20) instead of the smooth one shown in Fig. 13 and Fig. 14. In fact, Fig. 19 and Fig. 20 describes the estimation and control performances for both driver intervention and no driver one against more realistic crosswind effect. It is clear that these scenarios contain non-smooth variations of crosswind but the observer can capture the essence of crosswind effect in small error as shown in Fig. 19(a) and Fig. 20(a). Due to the action of motor assistance torque in Fig. 19(b), the driver consumed less steering wheel torque as seen in Fig. 19(c). Compared to the case of "No control"

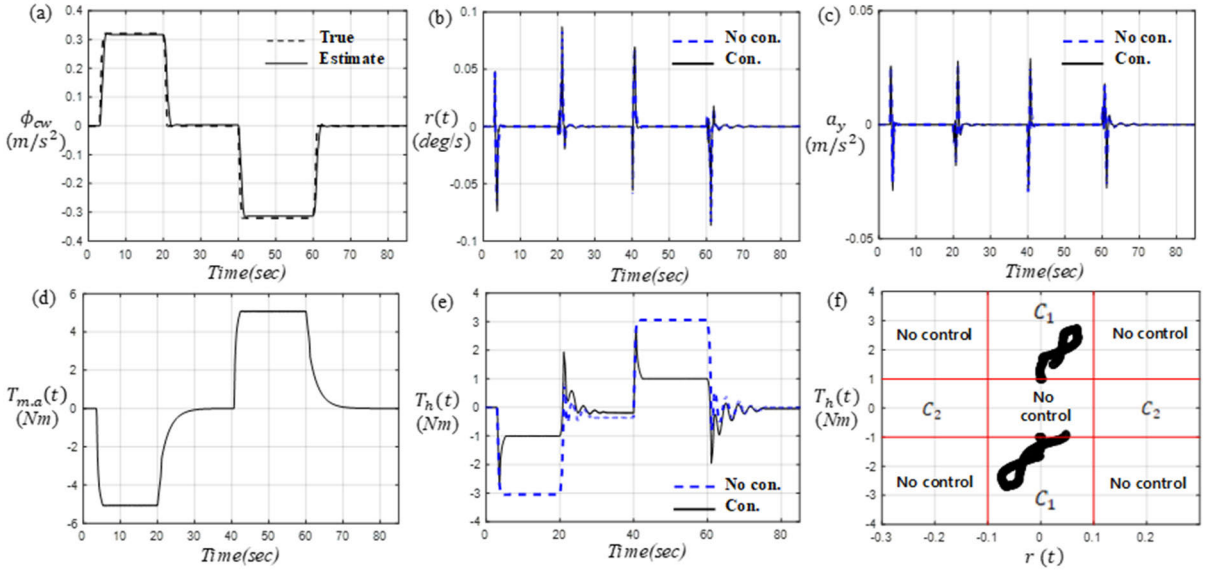

FIGURE 16. Estimation and control performances for the case with human driver intervention under the influence of crosswind effect (a) Estimates of ϕ_{cw}, (b) Yaw rate of vehicle $\mathbb{R}(t)$ (c) Lateral acceleration of vehicle a_y (m/s^2), (d) Assistance torque of motor $T_{m.a}(t)$, (e) Steering wheel torque $T_h(t)$, and (f) The trajectory of $\mathbb{R}(t)$ and $T_h(t)$ on the plane of selection condition.

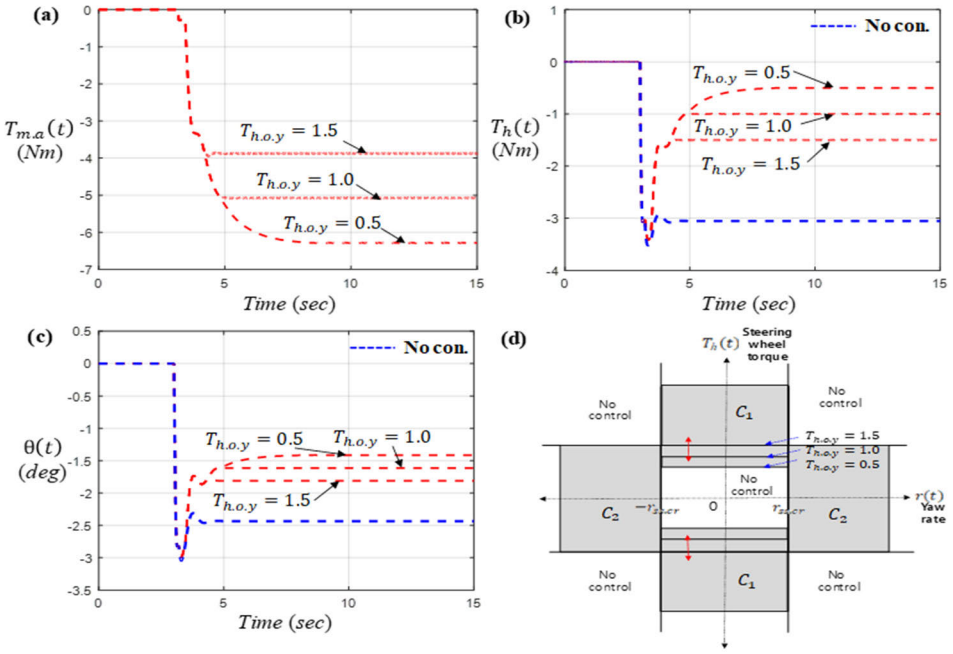

FIGURE 17. The consumed torques of both assistance motor and human driver according to the different level of $T_{h.o.y}$ in regions C_1 (a) Assistance motor torque $T_{m.a}(t)$, (b) Steering wheel torque $T_h(t)$, (c) Steering wheel angle and, (d) Tuned Control Mode Selection Conditions.

that driver should feel all variations of unwanted crosswind effect on the touch of steering wheel, the advantage of the proposed technique forces driver to maneuver the vehicle with the constant 1.1 Nm steering effort (even under non-smooth crosswind one). Meanwhile, Fig. 20 depicting the no driver intervention case indicates that both yaw rate and lateral acceleration of the vehicle have been reduced approximately 40% via the control system even under such unwanted effect. Moreover, the control performance for ''driver intervention'' case has been validated using a small HIL simulator (see Fig.21) originated from [13]. Two human test drivers are asked to steer the vehicle under the crosswind scenario shown in Fig. 22(a) and their steering efforts are described in Fig. 22(b) and (c). As predicted by the simulation results, it is apparent that both drivers applied constant and less steering wheel torques for this case. The results of Fig. 13 through

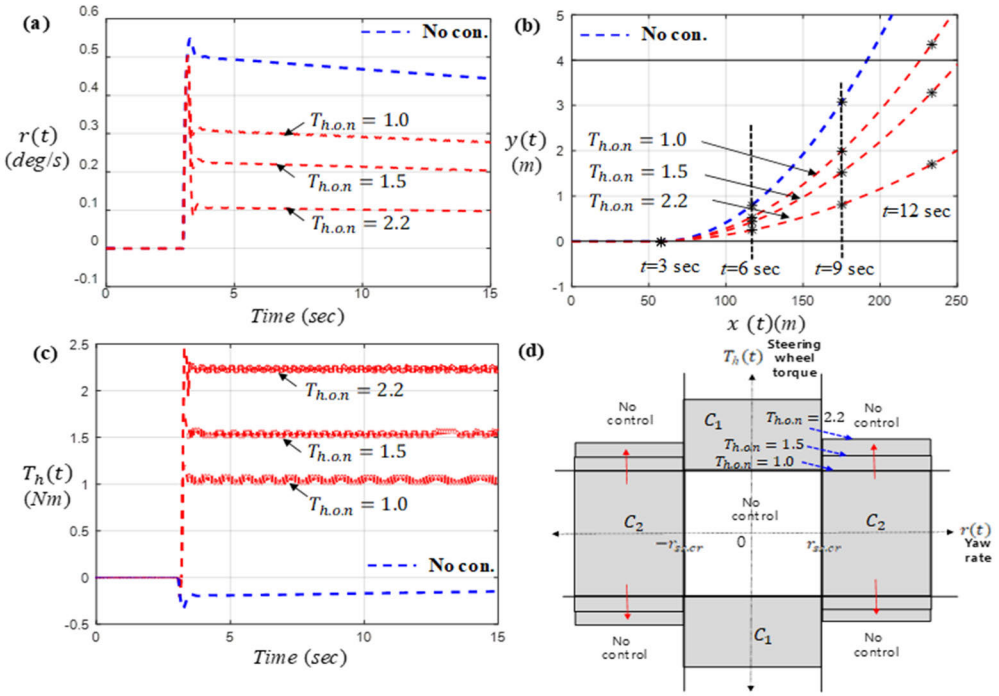

FIGURE 18. Control performances for the three expanded C_2 regions (No driver intervention) (a) Yaw rate of vehicle $\mathbb{R}(t)$ (b) The trajectory of vehicle (x(m) vs. y(m)), (c) Steering wheel angle and, (d) Tuned Control Mode Selection Conditions.

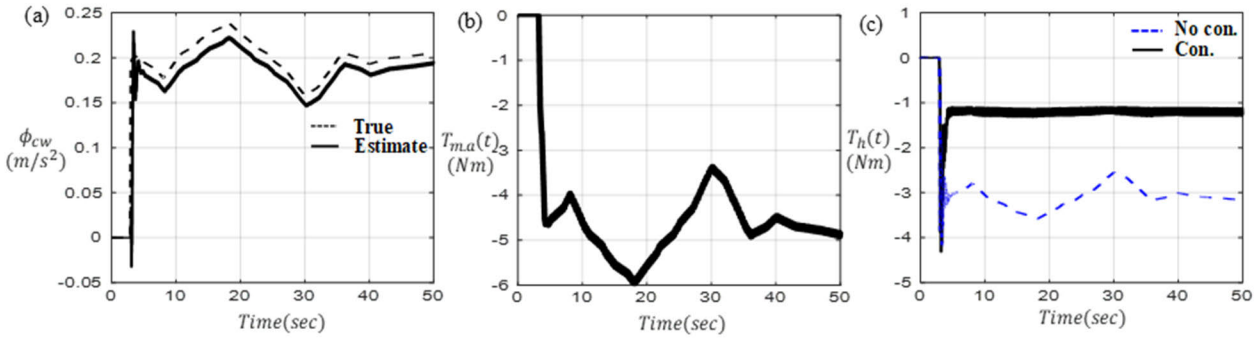

FIGURE 19. Estimation and Control performances for more realistic crosswind effect (driver intervention) (a) Estimates of ϕ_{cw}, (b) Assistance torque of motor $T_{m.a}(t)$ and (c) Steering wheel torque $T_h(t)$.

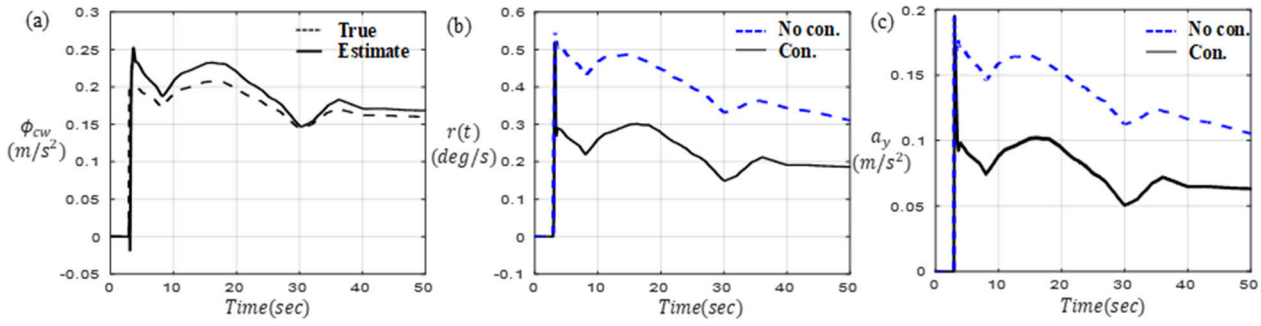

FIGURE 20. Estimation and Control performances for more realistic crosswind effect (No driver intervention) (a) Estimates of ϕ_{cw}, (b) Yaw rate of vehicle $\mathbb{R}(t)$ and (c) Lateral acceleration of vehicle a_y (m/s^2).

Fig. 22 show that the proposed disturbance observer estimates the unknown assumed crosswind effect and that the designed control strategy adequately conveys the control intention to the steering system for both cases.

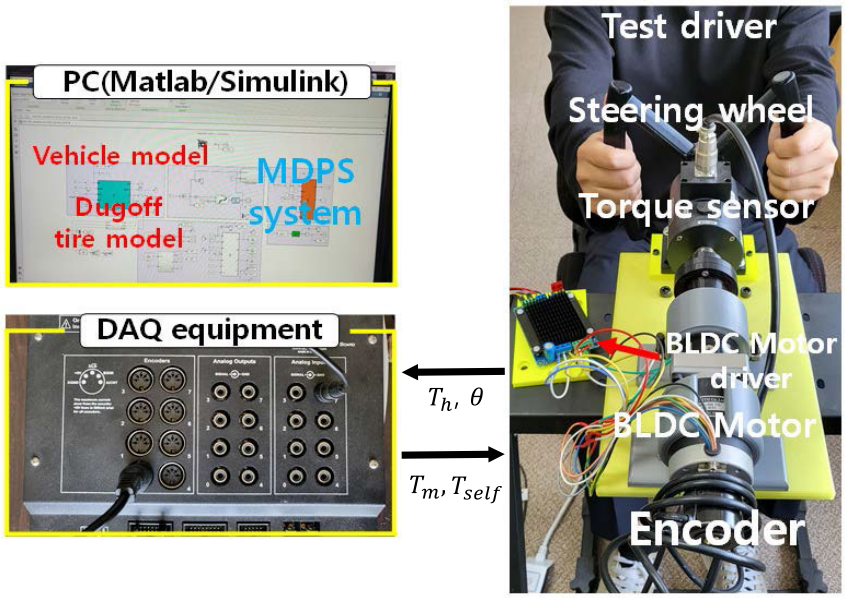

FIGURE 21. Hardware-In the-Loop-Simulation environment.

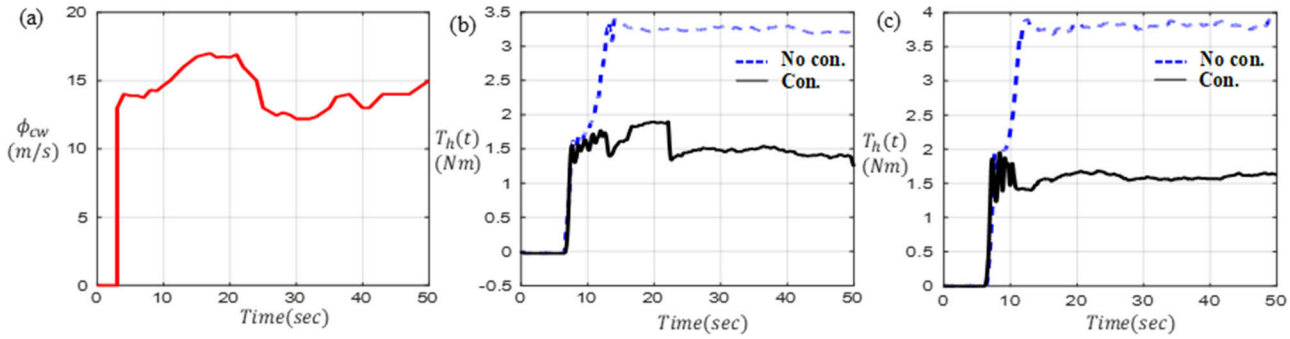

FIGURE 22. Control performances for the case of driver intervention in HILS (a) Scenario of crosswind effect (b) Steering wheel torque $T_h(t)$ for the 1st test driver and (c) Steering wheel torque $T_h(t)$ for the 2nd test driver.

VII. CONCLUSION

This paper proposed a novel compensation control strategy together with a disturbance observer for the crosswind effect. The disturbance observer is designed based on the extended state-space model and includes the adaptive estimation of disturbance. Meanwhile, the compensation control algorithm is equipped with two modes, the case with a driver intervention and the one without driver intervention, where we designed using the LQR approach considering a disturbance term and two different state-space models. In addition, the detection condition of crosswind and the control mode selection strategy between two controls are clearly addressed. The most advantage of the control strategy relies on the fact that the target steering effort (i.e, steering wheel torque) of a driver can be controlled resulting in the reduction of assistance motor torque or the decrease of undesired vehicle motion due to wind effect (i.e, efficient operation). Based on the Simulink/Carsim co-simulation and HILS environments, the effectiveness of the proposed estimation and control scheme has been evaluated according to several driving and crosswind scenarios. The unknown crosswind effect on the vehicle is successfully estimated with an appropriate detection time, while the control system assists the driver in terms of steering effort or reduces the crosswind impact on the vehicle. This work will be possibly another choice for the vehicle and automotive parts manufacturer when it comes to the lateral disturbance compensation control in their ADAS, without using vision based sensor for detecting the lane marker of road.

REFERENCES

[1] C. J. Baker and S. Reynolds, "Wind-induced accidents of road vehicles," *Accident Anal. Prevention*, vol. 24, no. 6, pp. 559–575, 1992.

[2] C. Wetzel and C. Proppe, "On reliability and sensitivity methods for vehicle systems under stochastic crosswind loads," *Vehicle Syst. Dyn.*, vol. 48, no. 1, pp. 79–95, Jan. 2010.

[3] C. J. Baker, "A simplified analysis of various types of wind-induced road vehicle accidents," *J. Wind Eng. Ind. Aerodynamics*, vol. 22, no. 1, pp. 69–85, 1986.
[4] R. G. Gawthorpe, "Wind effects on ground transportation," *J. Wind Eng. Ind. Aerodynamics*, vol. 52, pp. 73–92, May 1994.
[5] S. Glaser, S. Mammar, and D. Dakhlallah, "Lateral wind force and torque estimation for a driving assistance," *IFAC Proc. Volumes*, vol. 41, no. 2, pp. 5688–5693, 2008.
[6] K. Kim, S. Lee, and C. Park, "Estimation of lateral force due to lateral disturbance for application to an MDPS-based driving assistant system," *SAE Int. J. Mater. Manuf.*, vol. 4, no. 1, pp. 1014–1024, Apr. 2011, doi: 10.4271/2011-01-0977.
[7] K. W. Kim, S. B. Lee, C. S. Park, and K. Yi, "Estimation of lateral disturbance under parameter uncertainties," *Int. J. Automot. Technol.*, vol. 16, no. 3, pp. 427–433, Jun. 2015.
[8] J. B. Zhao, S. Y. Bei, and L. C. Zhang, "On reverse control strategy and anti-wind disturbance analysis of automotive EPS system," in *Applied Mechanics and Materials*. Trans Tech Publications, Nov. 2010, doi: 10.4028/www.scientific.net/amm.39.529.
[9] K. Kim, J. Choi, and K. Yi, "Lateral disturbance compensation using motor driven power steering," in *Proc. IEEE 75th Veh. Technol. Conf. (VTC Spring)*, Yokohama, Japan, May 2012, pp. 1–5, doi: 10.1109/VETECS.2012.6240282.
[10] K. Kim, B. Kim, Y. Go, J. Park, J. Park, I. Suh, and K. Yi, "An investigation on motor-driven power steering-based crosswind disturbance compensation for the reduction of driver steering effort," *Vehicle Syst. Dyn.*, vol. 52, no. 7, pp. 922–947, Jul. 2014, doi: 10.1080/00423114.2014.909941.
[11] B. Shao-yi, "Reverse assistance control and tests of electric vehicle EPS system under anti-wind interference condition," *Electr. Mach. Control*, 2012.
[12] S. Zhou, M. Zheng, F. Zhang, and M. Tomizuka, "Synthesized disturbance observer for vehicle lateral disturbance rejection," in *Proc. Annu. Amer. Control Conf. (ACC)*, Jun. 2018, pp. 398–403.
[13] D. Jung, "A minimally configured hardware-in-the-loop simulator of electrical power steering system for human driver interaction on crosswind effect," *IEEE Access*, vol. 9, pp. 60470–60481, 2021.
[14] (Jun. 25, 2014). *A Deep Dive Into Mercedes-Benz Crosswind Stabilization Technology | Video Inventory*. [Online]. Available: https://www.wagnermercedesofshrewsbury.com
[15] *Braced For Winter Storms: New Side Wind Stabilisation Tech Helps Ford Transits Stay in Lane Whatever The Weather*. Accessed: Nov. 14, 2022. [Online]. Available: https://media.ford.com/content/fordmedia/feu/en/news/2016/11/25/braced-for-winter-storms–new-side-wind-stabilisation-tech-helps.html
[16] S. Mammar, S. Glaser, and M. Netto, "Time to line crossing for lane departure avoidance: A theoretical study and an experimental setting," *IEEE Trans. Intell. Transp. Syst.*, vol. 7, no. 2, pp. 226–241, Jun. 2006.
[17] N. Katagiri, Y. Marumo, and H. Tsunashima, "Controller design and evaluation of lane-keeping-assistance system for motorcycles," *J. Mech. Syst. Transp. Logistics*, vol. 2, no. 1, pp. 43–54, 2009.
[18] A. Benine-Neto, S. Scalzi, S. Mammar, M. Netto, and B. Lusetti, "Model reference based vehicle lateral control for lane departure avoidance," *Int. J. Vehicle Auton. Syst.*, vol. 12, no. 3, pp. 284–306, 2014, doi: 10.1504/IJVAS.2014.063044.
[19] D. Hoehener, G. Huang, and D. D. Vecchio, "Design of a lane departure driver-assist system under safety specifications," in *Proc. IEEE 55th Conf. Decis. Control (CDC)*, Dec. 2016, pp. 2468–2474.
[20] S. Fankem, T. Weiskircher, and S. Müller, "Model-based rack force estimation for electric power steering," *IFAC Proc. Volumes*, vol. 47, no. 3, pp. 8469–8474, 2014.
[21] C. Dannöhl, S. Müller, and H. Ulbrich, "H∞-control of a rack-assisted electric power steering system," *Vehicle Syst. Dyn.*, vol. 50, no. 4, pp. 527–544, 2012.
[22] B. Jang, J. H. Kim, and S. M. Yang, "Application of rack type motor driven power steering control system for heavy vehicles," *Int. J. Automot. Technol.*, vol. 17, no. 3, pp. 409–414, Jun. 2016.

DAEYI JUNG received the Ph.D. degree in mechanical engineering from the University of Tennessee, Knoxville, USA, in 2012. He had worked as a Senior Researcher at Samsung Electronics and Hyundai Motors for several years. Since 2017, he has been with Kunsan National University, South Korea, where he is currently an Associate Professor with the Department of Mechanical Engineering. His research interest includes controls and analysis of nonlinear systems.

SORAM KIM received the bachelor's degree in mechanical energy engineering from Kunsan National University, South Korea, in 2021, where she is currently pursuing the master's degree in mechanical engineering. Her research interest includes vehicle dynamics and control.